



Review

Progress on the formation dynamics of the layered circulation in the South China Sea

Zhongya Cai^a, Jianping Gan^{a,*}, Zhiqiang Liu^b, Chiwing Rex Hui^a, Junlu Li^a^a Department of Mathematics and Department of Ocean Science, The Hong Kong University of Science and Technology, Hong Kong, China^b Southern University of Science and Technology, Shenzhen, China

ARTICLE INFO

Keywords:

South China Sea layered circulation
Formation dynamics
External vorticity flux
Intrinsic coupling
Stokes theorem

ABSTRACT

In the South China Sea (SCS), an alternating cyclonic-anticyclonic-cyclonic (CAC) circulation is recognized in the upper-middle-deep layers based on the principle of Stokes theorem. The CAC circulation is driven extrinsically by the East Asia monsoonal winds, a vertical sandwich-like inflow-outflow-inflow through Luzon Strait (LS) and intrinsically by the slope current-topography interaction. The understandings on the formation mechanisms of CAC circulation have been achieved based on different principles, and the physically solid interpretation on the CAC circulation need to be further clarified. In this paper, we review different dynamic perspectives from recent researches that describe the combined effects of surface wind forcing, lateral external forcing, and the intrinsic coupling among different layers. Our aim is to obtain a consistent understanding of the dynamics of the circulation in the SCS. The CAC circulation forms largely from the planetary vorticity flux that is extrinsically induced by the inflow-outflow-inflow through LS, which is predominantly balanced by the interaction between the CAC flow and bottom topography. Inside basin, the vertical motion dynamically links the circulation in three layers, and its spatial pattern has a strong impact on the basin circulation, particularly in the middle and deep layers. Vertical coupling of the layers occurs mainly over the slope because of the cross-slope motion due to interaction between strong slope current and topography. The internal layered circulation and intensified mixing, in turn, affect and maintain the layered current structure in LS. Based on the review of the forcing mechanisms, we offer perspectives for further investigations.

1. Introduction

The South China Sea (SCS) is the largest marginal sea in the tropics with a total area of $3.5 \times 10^6 \text{ km}^2$. It covers the region from the equator to 23° N and from 99° E to 121° E (Fig. 1). The central deep basin orients southwest to northeast and is bordered by two broad shelf regions in the north and south. The northern shelf locates to the south of China and extends southwestward from Taiwan to $\sim 13^\circ \text{ N}$. The southern shelf includes the Gulf of Thailand and Sunda Shelf between the Malay Peninsula and Borneo. There are no shelf regions in the eastern and western parts of the SCS, but with steep continental slope.

The SCS connects to the East China Sea through Taiwan Strait, to the Pacific Ocean through Luzon Strait (LS), to the Sulu Sea through Mindoro Strait, and to the Java Sea through Karimata Strait (Fig. 1). Of all the channels connecting the SCS to a surrounding sea, LS is the only deep water channel ($\sim 2500 \text{ m}$). Mindoro Strait is narrow with a sill depth of $\sim 400 \text{ m}$, while Taiwan Strait and Karimata Strait are shallower than 100 m . This unique topography defines the SCS a semi-

enclosed nature, which largely governs regional ocean dynamics of the SCS (e.g., Shaw and Chao, 1994; Xue et al., 2004; Liu et al., 2001; Yang et al., 2002; Gan et al., 2006) and of other marginal seas around the world.

The circulation in the SCS is largely driven by the East Asian monsoon and layered external flows from adjacent seas. These extrinsically forced currents interact with the slope topography and jointly determine the flow characteristics. The seasonal wind forcing is northeasterly in winter and has positive wind stress curl (WSC) prevails over the SCS basin (Liu and Xie, 1999). In summer, the wind forcing changes to westerly direction and WSC exhibits a dipole structure where positive/negative WSC is in the northern/southern part of basin.

In addition to the seasonal surface wind, the forcing by the time-dependent, three-dimensional water exchanges between the SCS and the adjacent oceans critically shape the circulation's characteristics. Fig. 2 shows how the transport through the straits around the SCS are spatiotemporally linked with each other and with the circulation in the SCS. Transport through LS provides the strongest external forcing for

* Corresponding author.

E-mail address: magan@ust.hk (J. Gan).

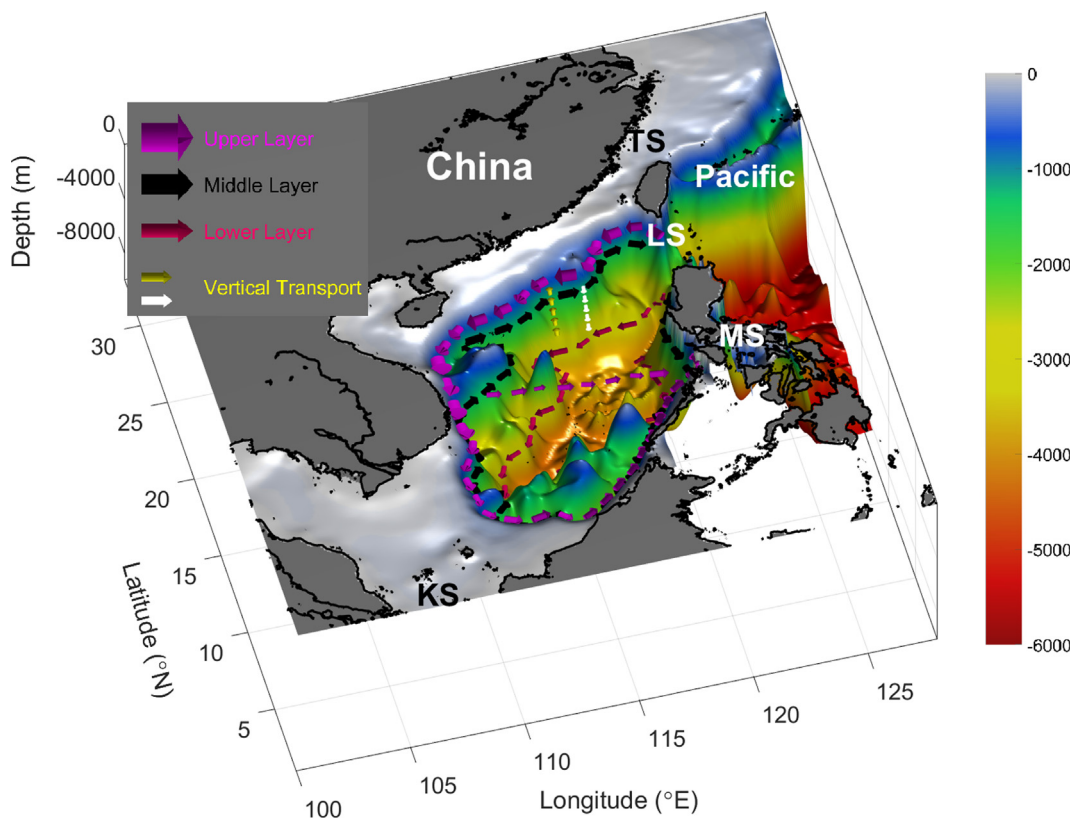


Fig. 1. Schematic annual mean CAC circulation in the South China Sea. Color contours represent bathymetry (m). LS: Luzon Strait; TS: Taiwan Strait; MS: Mindoro Strait; and KS: Karimata Strait.

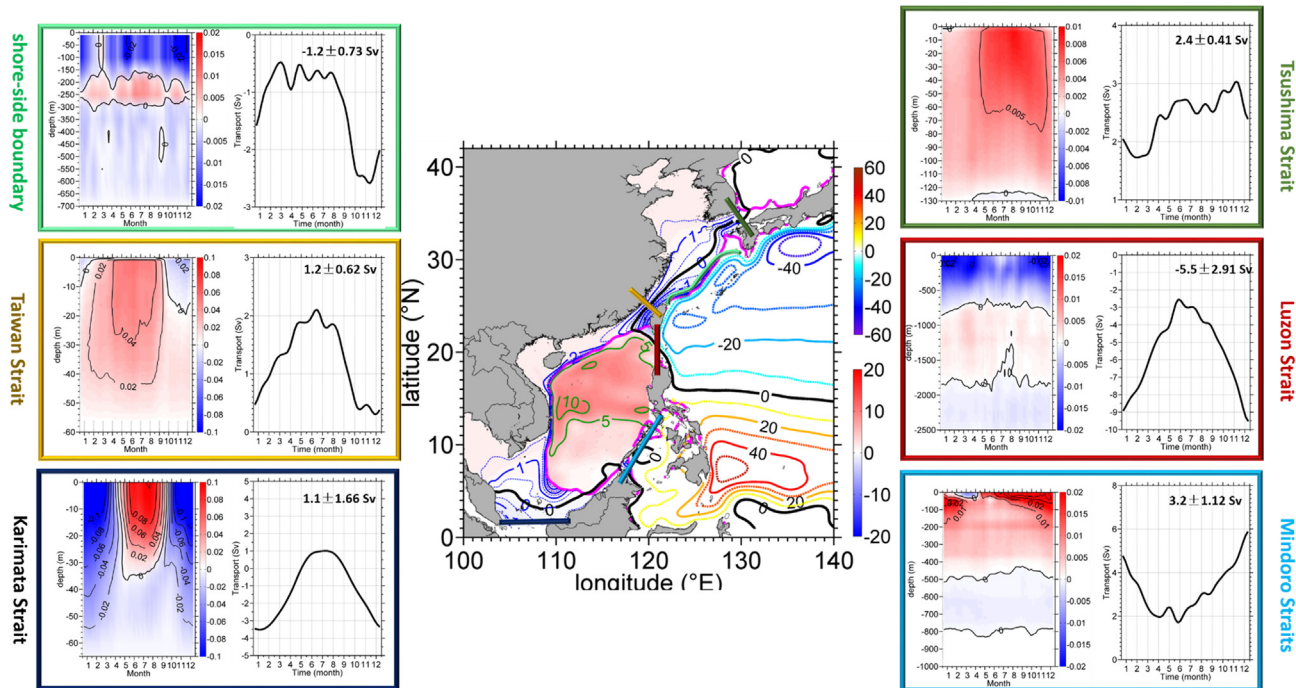


Fig. 2. Time series of depth-integrated transport (Sv) and depth-dependent mass flux ($10^6 \text{ m}^2 \text{ s}^{-1}$) through the straits around the China Seas (CS) and across the shore-side boundary (SSB) of the Kuroshio in the East China Sea. Each strait/SSB is indicated by a specific color bar and the result for each strait is shown in a box of the corresponding color. The background contours in the CS domain represent the annual mean transport stream function in the upper 750 m. The positive value refers to northward flows in Taiwan, Karimata, and Tsushima Straits, outflows in the Luzon and Mindoro Straits, and seaward flow along the SSB. The pink line represents the 200 m isobath. From Gan et al. (2016b). (For interpretation of the references to color in this figure legend, the reader is referred to the web version of this article.)

the basin's circulation. Based on long-term observations, LS transport is estimated as 3 to 6.5 Sv (e.g. Chu and Li, 2000; Qu et al., 2000; Liang et al., 2003; Su, 2004; Yaremchuk and Qu, 2004; Nan et al., 2013) and simulated values vary between 0.6 and 10.2 Sv (e.g., Lebedev and Yaremchuk, 2000; Metzger, 2003; Song, 2006; Yaremchuk et al., 2009; Zhao et al., 2009), as summarized in Hsin et al. (2012) and Nan et al. (2015).

The simulation by Gan et al. (2016b) estimates the coherently linked transports through four straits surrounding the SCS. They find that LS has a ~ 5.5 Sv westward intrusion (annual mean and water column-integrated) into the SCS from the Pacific Ocean. Then, conveyed by the slope of the SCS, ~ 1.2 Sv of the intrusive transport exits the basin through Taiwan Strait in the north, ~ 1.16 Sv exits through the Karimata Strait, and ~ 3.2 Sv exits through the Mindoro Strait in the south. The transport in LS shows strong seasonality, in which the inflow/outflow is weaker in summer and stronger during the other seasons. The variation of the transports is associated predominantly with the variable strength of the Kuroshio separation at the entrance of LS (e.g., Qu, 2000; Qu et al., 2005; Wang et al., 2006a, 2006b, 2006c; Gan et al., 2006; Wu and Hsin, 2012; Hsin et al., 2012) and with the interaction between the transports through the straits and the SCS circulation (Gan et al., 2016a).

The flux through LS has a prominent vertical sandwich-like structure which is seen in field observations and numerical model simulations (e.g. Chen and Huang, 1996; Tian et al., 2006; Fang et al., 2009; Yang et al., 2010; Zhang et al., 2010; Hsin et al., 2012; Nan et al., 2013; Gan et al., 2016a, 2016b). Pacific Ocean water intrudes into the SCS from upper and deep layers and the SCS water flows out of basin in the middle layer. It is conceivable that this sandwich structure is responsible for the layered circulation within the SCS because of vorticity influx or outflux.

The upper layer circulation in the SCS has been widely investigated using observed data (e.g. Wyrki, 1961; Shaw et al., 1999; Qu, 2000; Ho et al., 2000; Xie et al., 2013; Wang et al., 2006a, 2006b, 2006c; Rong et al., 2007; Cai and He, 2010) and numerical models (e.g., Bayler and Liu, 2008; Cai and Gan, 2017; Chern and Wang, 2003; Fang et al., 2005, 2009; Gan et al., 2006; Metzger and Hurlburt, 1996; Qu et al., 2004; Wei et al., 2016; Wu et al., 1998; Xue et al., 2004; Yang et al., 2002; Gan and Qu, 2008). The upper layer circulation has an annual mean cyclonic circulation pattern where there is a large cyclonic gyre in winter with a southwestward current along the continental margin in the northern and western part of basin. In summer, the circulation exhibits two kinds of patterns (Quan et al., 2016). In some studies, the upper layer shows basin scale anticyclonic circulation during summer (e.g. Chu et al., 1999; Xue et al., 2004; Fang et al., 2009), while other studies reveal a dipole structure with an cyclonic/anticyclonic gyre in the northern/southern basin (e.g., Su et al., 2004; Wang et al., 2006a, 2006b, 2006c; Cai et al., 2007; Quan et al., 2016; Gan et al., 2016b). The seasonal monsoonal winds and Kuroshio intrusion contribute to the annual mean cyclonic circulation pattern in the upper layer, but their relative importance and detailed mechanisms are not well-understood.

In the middle and deep layers, the characteristics of the circulation are poorly understood except for some qualitative or partially quantitative conjecture because of the lack of direct observations (Tian and Qu, 2012), and current knowledge is mainly based on numerical simulations and the limited observation data. The simulation by Yuan (2002) shows that there is a northward western boundary current centered at 500 m depth and a southward flow centered at 1000 m. Based on the mean of 18 years of output, Xu and Oey (2014) depict a robust vertically-averaged anticyclonic boundary circulation between 570 m and 2000 m depths, and below 2000 m, the circulation is cyclonic in the north and anticyclonic in the south. Based on temperature and salinity data from the U.S. Navy Generalized Digital Environment Model (GDEM), Wang et al. (2011) illustrate that a deep cyclonic circulation exists from about 2400 m to the bottom with westward, southward, and eastward currents along the northern, western, and

southern margins, respectively. Similarly, the analysis by Shu et al. (2014); based on HYCOM) and an analysis of GDEM data by Zhu et al. (2017) find that the current flows anti-cyclonically and cyclonically along the basin slope in the middle and deep layers.

The characteristic and detailed spatial pattern of the SCS circulation has been reviewed in literature but most articles focused on the circulation in a specific layer or certain phenomenon without looking at the layered circulation holistically within the full water column (e.g., Qu et al., 2009; Fang et al., 2012; Hu et al., 2000; Su, 2004; Liu et al., 2008; Tian and Qu, 2012; Wang et al., 2016). Recently, Zhu et al. (2019) overview the circulation in the SCS layer by layer and outline some possible forcing mechanisms. However, this work emphasizes mainly on the characteristics of the circulation in each layer and do not physically clarify the relationship and discrepancies among different mechanisms, which is crucial to advance our knowledge on the dynamics realization of circulation in the SCS. Similarly, Wang et al. (2019) review the internal wave, internal tide and solitary waves in SCS and their influences in the mixing and CAC circulation, but still do not integrate various forcing mechanisms during the formation and sustenance of the CAC circulation. In addition, the vertical partitions of the circulation have not been physically validated. Thus, the vertical structure and the intensity of the CAC circulation still need to be physically clarified.

The knowledge of the CAC dynamics is crucial to understanding and validating the circulation. From the past studies, the theoretical understandings on CAC circulation have been achieved that the three-layer inflow-outflow-inflow through LS induces the positive-negative-positive vorticity flux in the respective layers to form the CAC circulation, which, however, are developed from differing principles and explain the basin circulation from different perspectives. The sign of the vorticity/potential vorticity (PV) flux induced by the inflow varies in different studies, in this review the influx of vorticity/PV is defined as positive. Thus, we still require a physically consistent understanding of the layered circulation in the SCS. Moreover, the coupled dynamics between the intrinsic processes and external forcing in the CAC circulation are still not well understood and is an on-going research topic.

In this paper, we review and discuss the identification of layered circulation, the theoretical understanding of the forcing mechanisms, and the relationships and discrepancies among the different approaches. Our objective is to obtain a consistent understanding of the dynamics of the circulation in the SCS. The paper is organized as follows: Section 2 discusses the vertical partition of the CAC circulation; Section 3 reviews the driving mechanisms of the CAC circulation and discusses the relationship and discrepancies; Section 4 discusses the vertical coupling among different layers; and, finally, Section 5 provides conclusions and future prospects.

2. The vertical partitions of the CAC circulation

The layered CAC circulation pattern in the SCS is well-recognized in the literature, but much of the research focused on the horizontal circulation at a specific depth or on a vertical transect off the western boundary. Moreover, these studies did not provide a holistic perspective of the structure or the pathways of the flow in the three-dimensional CAC (e.g. Yuan, 2002; Li and Qu, 2006; Shu et al., 2014; Zhu et al., 2017).

The numerical study by Yuan (2002) illustrates that the southward western boundary current is centered at 200 m and 1100 m depths, and the northward current is centered at 500 m depth. The vorticity balance of the circulation is between the vortex stretching and the meridional change of the planetary vorticity. Similar results are presented by other numerical simulations (e.g. Xu and Oey, 2014; Shu et al., 2014), most of which identify the circulation in the basin based on eye views of the localized vortex or the western boundary current. The definitions of the circulation in those numerical studies are arbitrary and deterministic, and the vertical partition of the CAC circulation cannot be quantitatively identified.

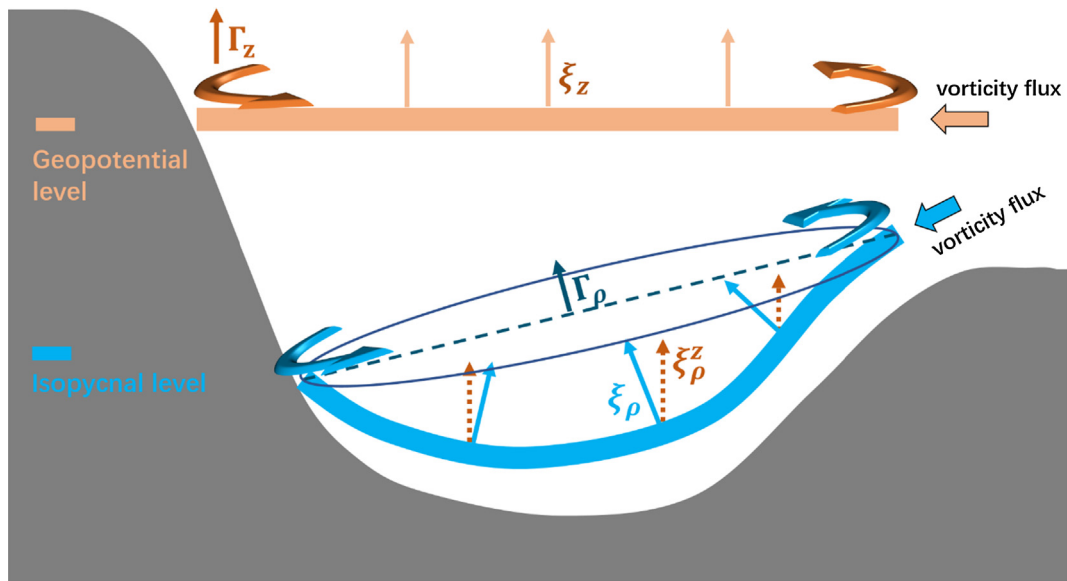


Fig. 3. Conceptual diagram of the vorticity, ξ , and basin circulation, Γ , in geopotential (with subscript z) and isopycnal (with subscript ρ) levels. ξ_ρ^z represents the vertical component of the relative vorticity (ξ_ρ) in the isopycnal level.

For basin-scale rotational circulation, a more physically valid explanation of circulation direction is based on Stokes theorem:

$$\Gamma = \oint \vec{V} dl = \iint \zeta dA, \quad (1)$$

where Γ is the basin circulation; \vec{V} is the velocity vector; and ζ is vertical relative vorticity normal to A , which is the area of the inner basin. Because the contribution to the CAC circulation is composed by the sum of organized, but different, circulation hotspots over the basin, Γ may be qualitatively and quantitatively different from a subjective identification based on a top view of the flow field.

Eq. (1) provides a physically valid way of quantifying the intensity and structure of the layered circulation in the SCS. The layered circulation at each geopotential level that satisfies Stokes theorem (Γ_z in the vertical direction in Fig. 3) is calculated so that the vertical structure and intensity is known. Using Eq. (1), Gan et al. (2016a) firstly provide a vertical profile of the rotating CAC circulation in the SCS. Fig. 4 shows that the three layers in the CAC are vertically separated by the 750 m and 1500 m depths. Previous estimates of the vertical partition of the

three layers are similar; for example, separated by 500 m and 1700 m in Li and Qu (2006) and by 570 m and 2000 m in Xu and Oey (2014).

Fig. 4 also displays the seasonality of the CAC circulation. The cyclonic circulation in the upper layer is stronger in winter driven by northeasterly wind forcing with positive WSC and a stronger winter Kuroshio intrusion (e.g., Qu, 2000; Gan et al., 2006). However, the upper layer circulation in summer features a dipole pattern, thus the domain-integrated positive vorticity is relatively small. It also illustrates that the thickness of the upper layer circulation is thinner in summer and thicker in winter. Unlike the flow pattern in the upper layer, the anticyclonic and cyclonic circulations in the middle and deep layers are more intense in summer than in winter. Furthermore, the location of the middle layer is shallower in summer than in winter.

The basin circulation can also be interpreted using isopycnal level and the circulation over isopycnal surfaces is physically sensitive to depict the forcing mechanisms of the CAC circulation. Previous studies in SCS have attempted to provide the basic velocity pattern in density level. For example, according to calculated the θ/S and σ_θ/S diagrams, Wei et al. (2016) define the subsurface, intermediate, and deep layers of the isopycnal surfaces as $25.0 \sigma_\theta$, $26.7 \sigma_\theta$, and $27.6 \sigma_\theta$, respectively. Similarly, Zhu et al. (2017) derive the geostrophic velocity from GDEM3.0 hydrographic data and interpret the sandwiched circulation in density layers. Zhu et al. (2017) separate three layers by the $26.4 \sigma_\theta$ and $27.62 \sigma_\theta$, which is based on the meridionally averaged zonal velocity in LS and calculated the layered-averaged vorticity in the three density layers. The density layer averaged circulation patterns are calculated in those studies, however, the quantitative and physically valid vertical profile of basin circulation as a function of potential density has not been provided in the SCS research now.

As illustrated in Fig. 3, to depict layered circulation using isopycnal surfaces and Stokes theorem, the vertical vorticity (ξ_ρ^z) needs to be converted to the vorticity perpendicular to an isopycnal surface (ξ_ρ). As a result, Γ_ρ represents the circulation over the “averaged” isopycnal surface. Because the depth of the isopycnal surface tilts against the geopotential surface and changes over the basin, Γ_ρ and ξ_ρ do not have a consistent direction in the basin within the different isopycnal levels, and they may exhibit different patterns from that in the geopotential level. Thus, Γ_ρ defined over the isopycnal surface might not represent the layered horizontal circulation because it includes the circulation from other directions (Fig. 3).

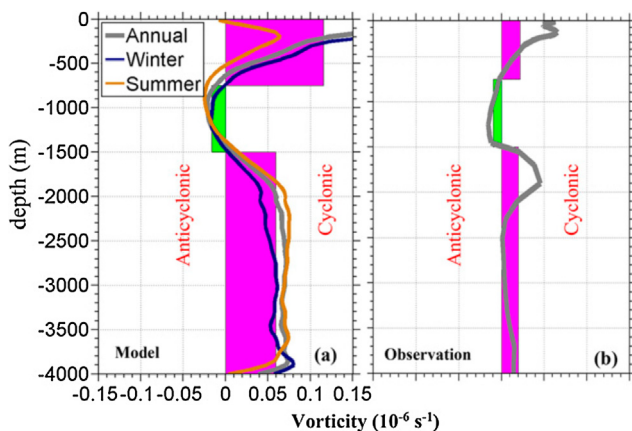


Fig. 4. Domain-averaged annual- and seasonal-mean vorticity as a function of depth from (a) model results and (b) annual-mean geostrophic current velocities derived from GDEM hydrographic data. Green (negative) and purple (positive) bars are the averaged vorticity in the specific layers. From Gan et al. (2016a). (For interpretation of the references to color in this figure legend, the reader is referred to the web version of this article.)

3. Driving mechanisms of CAC circulation

3.1. External forcing

External forcing from winds, tides, and the intrusion of the Kuroshio through LS are critically important to the SCS layered circulation. While the effects of wind forcing are relatively well-known, uncertainties remain about the influences of the tides and the intrusion of the Kuroshio. The intrusion is closely linked to the current system in the tropical western Pacific Ocean that involves the North Equatorial Current (NEC) and its downstream components, the Kuroshio Current (KC) and Mindoro Current (MC). This section details the effects of tidal mixing and the KC intrusion on the SCS circulation

(a) NEC-KC-MC system in the tropical western Pacific system

In the Western Pacific Ocean, the NEC flows westward from 8°N to 18°N with the center located around 13°N under the prevailing easterly trade wind. Vertically, the bottom of the NEC reaches ~ 500 m and deepens poleward. It carries ~ 50 Sv of water into the warm pool and feeds into the mid-latitude and equatorial regions through the KC and MC, respectively (e.g., Nitani, 1972; Qiu and Lukas, 1996; Qu et al., 1998; Toole et al., 1988; Toole et al., 1990). The KC and MC are the warm, deep, swift western boundary currents downstream of the NEC. Their annual mean volume transports exceed 20 Sv with the MC being stronger than the KC (e.g., Kashino et al., 2009; Qiu and Lukas, 1996; Qu et al., 1998; Tozuka et al., 2002; Wijffels et al., 1995; Gan et al., 2016b).

The seasonal variation of the NEC-MC-KC system has been investigated widely. The strength of the KC determines the heat and water distribution at mid-latitudes, which is critical to the circulation in SCS. Generally, the NEC is strong in spring/summer and weak in autumn (e.g., Gan et al., 2016b; Qu et al., 1998; Tozuka et al., 2002; Yaremchuk and Qu, 2004). Meanwhile, the NEC bifurcation stays in the south in spring/summer and shifts northward in autumn (e.g., Kim et al., 2004; Qu and Lukas, 2003). The stronger NEC and southward movement of the bifurcation result in an intensified KC in spring and summer and a weaker KC in autumn.

As the KC encounters LS, the KC's main flow passes through the strait and partially intrudes into the SCS at Balintang Channel (Chern and Wang, 1998; Liang et al., 2003; Gan et al., 2006). The net intrusive transport and flow patterns closely link to the strength of the upstream KC (e.g. Caruso et al., 2006; Gan et al., 2016b; Nan et al., 2015). Like the main KC's intensity, KC intrusion exhibits a seasonality that it is strong in winter and weak in summer. It is suggested that the weak intrusion in summer is due to the stronger main KC (Caruso et al., 2006; Gan et al., 2006). While in autumn and winter, the weaker KC leads to an anti-cyclonic looping current that penetrates the SCS before returning to the main KC, which provides more intrusive water (Caruso et al., 2006).

(b) Tidal forcing and mixing

The SCS has extensive internal tides (Kantha and Tierney, 1997) and tidal mixing. The estimated internal tidal energy flux generated in LS and radiating into the SCS is 7 to 10 GW (e.g. Jan et al., 2008; Niwa and Hibiya, 2004; Tian et al., 2009; Alford et al., 2015). Most of the imported energy eventually dissipates in the SCS (Zhao, 2014) and notably amplifies the turbulent mixing (Alford et al., 2015). It is observed that the turbulent mixing rate in the SCS is several orders of magnitude larger than that in the North Pacific Ocean (NPO) (Tian et al., 2009; Wang et al., 2016; Yang et al., 2019). The turbulent mixing intensity increases with depth and reaches on the order of $10^{-2} \text{ m}^2 \text{ s}^{-1}$ in the deep layer (Yang et al., 2016). The contrasting intensity of the mixing in the deep waters on both sides of LS drives the water exchange between the SCS and the NPO (e.g. Zhao et al., 2014; Wang et al., 2017),

possibly through maintaining the eastward density gradient across the deep layer of LS (Qu et al., 2006). Inside the basin, tidally-induced energy dissipation, amplified over a rough slope topography with complicated seamounts and canyons in the northern SCS (Chang et al., 2006), is one of the key mechanisms that alter the cross-layer exchange of momentum and water masses and the vertically interlinked CAC circulation in the northern SCS (Liu and Gan, 2017). The complex slope topography causes the variability of the internal tide's energy dissipation rate and the associated turbulent mixing in the SCS (Wang et al., 2016).

Regional high-resolution numerical simulations are used to investigate the overall characteristics and behavior of barotropic and baroclinic tides (e.g. Jan et al., 2008; Niwa and Hibiya, 2004; Alford et al., 2015). Zu et al. (2008) propose that the response of the tides in the SCS are critically determined by the propagating direction of tides in the NPO and regional geometry and topography. Fang et al. (1999) draw a similar conclusion. The prominent sill-like topography in LS enhances conversion of barotropic tidal energy to baroclinic modes (e.g. Niwa and Hibiya, 2004; Jan et al., 2008). Because baroclinic processes or background flow, like the Kuroshio and the CAC circulation, are removed in the most numerical tidal simulations, those simulations are not holistically configured to resolve the complete dynamics of the background flow or the barotropic and baroclinic tides (Guo and Chen, 2014).

The importance of the multi-scale background flow, especially the Kuroshio, in altering the behavior of the internal tides and diapycnal mixing in the SCS is recently re-emphasized by many researchers such as Jan et al. (2012), Yang et al. (2014), Alford et al. (2015), and Liu et al. (2015). The Kuroshio intrusion in LS can regionally elevate the diapycnal diffusivity in the mixed layer and the pycnocline with its augmented shear instability (Yang et al., 2014), and strengthen the internal tides during winter (Liu et al., 2015). Alford et al. (2015) also found that the Kuroshio noticeably refracts the internal wave field emanating from LS, and profoundly alters the inclination angle and propagation path of internal tides in the SCS. However, due to a poorly simulated Kuroshio and CAC circulation, the influence of the Kuroshio on the internal tides is still not well-resolved, as summarized by Guo and Chen (2014). Thus, the interaction of tidal and sub-tidal dynamics in the SCS layered circulation is still an open question.

In the simulation of tidally- and subtidally-driven circulation in the SCS, the tidal and sub-tidal forces are imposed inconsistently along the open boundary of the computational domain. The prescribed elevation/current along the open boundary is known to worsen the tidal and sub-tidal flows, although this kind of configuration is widely used. By decomposing the disturbances imposed by tidal and sub-tidal forces, Liu and Gan (2016) propose a possible solution by implementing a novel open boundary condition in the Regional Ocean Modeling System (ROMS). Their scheme plays a critical role in reconstructing the sensible circulation for both tidal and sub-tidal components in the China Sea Multi-Scale Ocean Modeling System (CMOMS, <https://odmp.ust.hk/cmoms/>) by Gan et al. (2016a and 2016b).

3.2. Adjusting and establishing the upper layer circulation

Seasonal wind forcing largely drives the upper layer SCS circulation and its seasonality. In the open ocean, the basin achieves Sverdrup balance when the forced Rossby wave plus the free Rossby wave balance the WSC (Anderson and Gill, 1975). For the circulation dynamics in the upper layer of the SCS, due to the relatively small basin size, the planetary wave crosses the SCS basin within 1 to 4 months at wave speeds of 10 to 40 cm/s. The corresponding relatively short thermocline adjustment time implies that local variability does not dominate over the forcing at annual scales. Instead, the response of forced planetary wave to the seasonal wind forcing degenerates to a quasi-steady state.

When a wind stress is imposed over the SCS, the barotropic Rossby waves rapidly cross the basin in several days and leave a barotropic

Sverdrup flow (Pedlosky, 1996) with little vertical shear:

$$\beta \partial_x \Psi = \nabla \times \left(\frac{\vec{\tau}_s}{\rho_0} \right), \quad (2)$$

where Ψ is the total transport streamfunction for flows integrated over the entire water column. Then after the first baroclinic wave crosses the basin, the abyssal flow diminishes and the transport concentrates only in the upper ocean. Consequently, the complete Sverdrup relationship in Eq. (2) reduces to the upper ocean baroclinic Sverdrup balance:

$$\beta H v_g = f w_e \quad (3)$$

where v_g is the thermocline flow, and $w_e = \nabla \times (\vec{\tau}_s / \rho_0 f)$ is the Ekman pumping velocity. Now, the flow is strongly baroclinic and the resulting baroclinic sea surface height is the dominant component. The ratio between the baroclinic flow and the barotropic flow is estimated by D_0/H , where D_0 is the depth of ocean bottom, and H is the mean thermocline depth. This interpretation is supported by the results of a reduced-gravity ocean model in a closed basin (Cessi and Louazel, 2001). With time-dependent wind forcing, the reduced-gravity model shows that the ocean has an amplified response with a period equivalent to the transit time required for a long Rossby wave to cross the basin.

In addition to the Rossby waves, the abyssal circulation shows propagating Kelvin waves as a response to deep water formation (e.g. Kawase, 1987; Cane, 1989). Similarly, the spin-up and adjustment of the upper layer circulation respond to the forcing with cyclonically propagating Kelvin waves along the basin boundary as well with periods less than a few months (e.g. Yang, 1999; Johnson and Marshall, 2002; Marshall and Johnson, 2013). When travelling along the eastern boundary, it radiates the Rossby waves that propagate westward into the interior. In the SCS, the model simulation (Wang et al., 2003) describes the similar Kelvin wave propagation during the establishment of upper layer circulation.

The above studies focus on the region's dynamics respond to wind forcing in the SCS. They elucidate how the upper layer circulation adjusts to wind forcing but ignore the external forcing through LS. The sensitivity experiments by Liu et al. (2001) show that the inclusion of the Kuroshio intrusion improves the simulated SSH anomaly in the northern SCS. Xu and Oey (2015) illustrate that the LS intrusion accounts for 38% of SSH variability in the northern SCS, and the intrusion alters the forced Rossby wave response. Without inclusion of the intrusion, westward propagation of the Rossby wave would be too fast and results in an incorrect dynamic balance and erroneous annual SSH variability in the northern SCS.

3.3. Source-sink driven abyssal circulation

Stommel and Arons (1959) investigate the abyssal flow pattern driven by a mass source-sink distribution. They sketch the flow patterns for various source/sink distributions and meridional and zonal boundary conditions based on the linearized dynamical equation of a homogeneous layer of fluid:

$$\begin{aligned} \frac{\partial \vec{V}_H}{\partial t} + f \vec{k} \times \vec{V}_H &= -g \nabla_H \eta \\ \left(\frac{\partial \eta}{\partial t} + Q \right) + \nabla_H \cdot (h \vec{V}_H) &= 0 \end{aligned} \quad (4)$$

where η is the displacement of the free surface and Q is the upward passage of water through the free surface. In a steady state, the solution of \vec{V}_H and η are obtained from the given water depth (h), distribution of source/sink (Q), and boundary conditions. Driven by the centered mass source and a spatially uniform mass sink Q , there is a stronger western boundary current directing from the source region to the sink region and a weaker interior flow in the opposite direction.

Stommel and Arons' classic theory provides the quantitative

patterns of basin circulation and has been applied in studies to understand the circulation in the SCS, especially in the deeper layers (e.g. Yuan, 2002; Zhu et al., 2017; Zhou et al., 2017). The deep intrusion from LS can be regarded as the mass source and is balanced by an upward mass flux (advection and mixing processes), thus the deep basin should have a relatively strong southward western boundary current with a northward interior flow in the central basin. Following this theory, Yuan (2002) shows the balance between the vertical vortex stretching and the vorticity induced by the movement within the planetary vorticity gradient; that is, $f \frac{dw}{dz} = \beta v$. This balance holds for the majority part of the water column in a central basin region.

However, the simplified theory described by Eq. (4) ignores the nonlinear advection and frictional effects. The equation helps to understand the circulation pattern in a closed basin, but it cannot provide the full dynamics of the SCS basin circulation in response to external forcing of the mass source/sink.

3.4. Potential vorticity conservation constraint

Above discussion provides a useful theoretical framework for understanding the circulation patterns in the SCS but focuses on the particular processes without addressing the details of the layered circulation. It cannot link different forcing factors nor quantified the coupling dynamics of the internal processes and external forcing in the CAC circulation.

Following the work of Stommel and Arons (1959) and Kawase (1987), Yang and Price (2000) further develop the theory of the source/sink driven circulation and obtain PV constraints based on a one-layer reduced gravity momentum equation:

$$\sum_{i=1}^N \frac{Q_i f_i}{H_i} = -\lambda \oint_c (\vec{u}_h \vec{l}) ds \quad (5)$$

where Q_i is the volume transport through the straits of the basin. f_i and H_i are the Coriolis parameter and the mean layer thickness at the i -th opening. λ is the Rayleigh friction coefficient. $\vec{u}_h = (u, v)$ is the horizontal velocity vector. \vec{l} is the unit vector tangential to the lateral boundary. Eq. (5) indicates that, in steady state, the net PV influx through the straits into a density layer is balanced by friction-induced PV dissipation. Thus, the net influx/outflux of PV generates cyclonic/anticyclonic basin circulation with negative/positive friction curl. By adding terms that represent the frictional effect on the surface, the WSC is included. Thus, the bottom friction dissipates the net PV influx and the WSC input in the upper layer:

$$\sum_{i=1}^N \frac{Q_i f_i}{H_i} + \nabla \times \left(\frac{\vec{\tau}_s}{H} \right) = -\lambda \oint_c (\vec{u}_h \vec{l}) ds \quad (6)$$

where $\vec{\tau}_s$ is the surface wind stress. Eq. (6) illustrates the basic response of basin circulation to external forcing and can identify the direction of circulation in the upper layer. In the SCS, Eq. (5) is adopted to investigate the formation of deep layer circulation and its seasonality (e.g. Lan et al., 2013; Xu and Oey, 2014; Lan et al., 2015). However, Eq. (5) is for a single layer, and it ignores the linkages among different layers that are important for maintaining the CAC circulation (see Section 4). It should be noted that when applying this PV constraint, the friction term in Eq. (5) may not reflect the net interfacial stress, particularly in the vertical alternating three layer circulation in the SCS.

Similarly, based on Pedlosky (1998), Zhu et al. (2017) derive the potential vorticity equation using four-and-a-half-layer quasi-geostrophic model in density layer (Fig. 5) to explore the contribution of the lateral PV flux on the layered circulation in the SCS:

$$\begin{aligned} \lambda \oint_c (\vec{u}_h \vec{l}) dl \\ = \frac{f_0}{H_n} (QD_{Z_n} - QD_{Z_{n+1}}) - \int_{ba \sin} (\vec{u} \cdot \vec{n}) q_n dl - \sum_{i=1}^K \frac{QL_n f_i}{H_{ni}} + \Delta Q, \end{aligned} \quad (7)$$

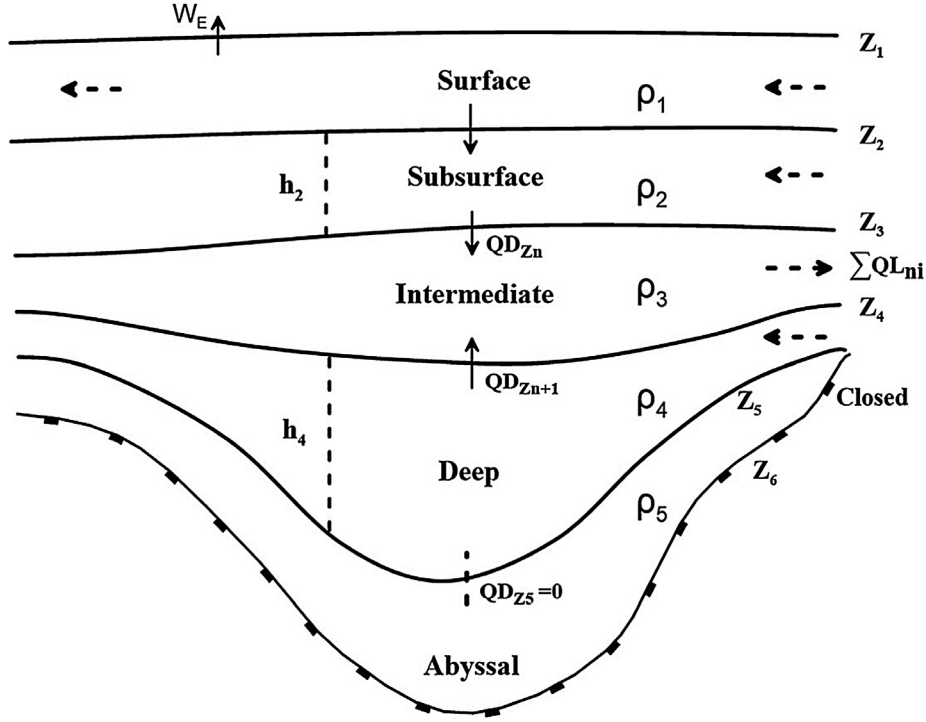


Fig. 5. Schematic presentation of a 4-1/2 layer quasi-geostrophic model. The upper interface of the n th density layer is at $Z = Z_n$, varying with (x, y) , and its thickness is $h_n = Z_n - Z_{n+1} = H_n + \delta h_n$. The lateral boundary is closed in the abyssal layer. From Zhu et al. (2017).

where H_n is the horizontally averaged value of the layer thickness; q_n is the quasi-geostrophic approximation of the full form of the potential vorticity; and f_0 is the constant value that indicates the typical Coriolis parameter of the SCS. QD represents the vertical crossing diapycnal volume flux and QL is the lateral volume flux through the opening in the given layer. The equation implies that in density layers and in steady state, the basin boundary circulation, on the left hand side of the equation, is controlled by the cross-interface vorticity, cross-integration-circuit vorticity, lateral potential vorticity flux and the rest baroclinic vorticity terms, respectively. In the special case of one-layer flow, Eq. (7) degenerates into Eq. (6).

Zhu et al. (2017) find that the lateral PV flux is the primary driver of the layered circulation. For the other terms, the cross-interface and cross-integration-circuit vorticities, with decreasing importance with depth, are of the same order as the lateral PV flux in the subsurface and intermediate layers, but one order magnitude smaller in the deep layer. On the contrary, the baroclinic induced terms, with increasing importance with depth, are of the same order as the lateral PV flux in the intermediate and deep layers, but much smaller in the subsurface layer.

The abyssal SCS below ~ 2500 m is a closed basin that has no direct external vorticity flux from the surrounding straits. Some studies (e.g. Xu and Oey, 2014) speculate that there is no net circulation in the abyssal SCS and the cyclonic circulation in one region must be compensated by anticyclonic circulation somewhere else. However, according to Xie et al. (2013) and Wang et al. (2011), the circulation pattern at 3000 m, or below 2400 m, in the SCS is cyclonic. Gan et al (2016a) also show there is strong net cyclonic circulation in the deep ocean below 2500 m. The PV dynamics in Eq. (7) could provide an easy explanation that, according to the layer partition in Zhu et al (2017), the density layer between $27.62 \sigma_\theta$ and $27.66 \sigma_\theta$ extends to most of the deep basin below 2500 m. Thus, the cyclonic circulation between these two isopycnal surfaces is driven by the lateral PV flux in the same density layer through LS. This issue can also be explained by the vorticity dynamics at the geopotential level as we discuss in Section 3.4.

Although Eqs. (6) and (7) diagnose the direction of the basin circulation and explain the cyclonic circulation in the abyssal basin, the

variables in these equations are depth-independent within the layer, which may not be suitable for the vertical varying CAC circulation (Fig. 4). Besides, the final balance is between the influx of PV and the bottom friction curl and does not explicitly show the topographic effect, which is crucial to interpreting the intrinsic physical processes that modulate the structures of the slope current and basin circulation in the SCS with broad slope topography. Moreover, when the density layer meets the bottom topography, the thickness and the horizontal range of the density layer would be affected by the bottom topography when the isopycnal surface oscillates vertically. This may induce difficulties like discontinuity issues when the PV balance constraint is applied to the density layer. Thus, the model with outcropping is adopted to handle the grounding phenomenon in studies that use layered model (e.g., Wang et al., 2018).

3.5. Depth-integrated vorticity dynamics

To identify the multi-forcing of winds, lateral fluxes, and intrinsic dynamics of the flow-topography interaction, Gan et al (2016a) uses the domain- and depth- integrated vorticity balance for each layer:

$$\begin{aligned} \int_A [\nabla \times \vec{V}_i] dA = & - \int_A \left[\nabla \times \int_{L_b}^{L_u} \widehat{HNL} dz \right] dA - \int_A \left[\nabla \times \int_{L_b}^{L_u} \widehat{VNL} dz \right] dA \\ & + \int_A \left[\nabla \times \int_{L_b}^{L_u} \widehat{PGF} dz \right] dA \\ & - \int_A [\nabla \cdot \widehat{fV}] dA + \int_A \left[\nabla \times \int_{L_b}^{L_u} \widehat{VVIS} dz \right] dA + \int_A \left[\nabla \times \int_{L_b}^{L_u} \widehat{HVIS} dz \right] dA \end{aligned} \quad (8)$$

where the terms L_u and L_b are the depths of the top and bottom of each layer, respectively. A is the domain of the basin. u and v are the velocities in zonal (x) and meridional (y) directions, respectively. f is the

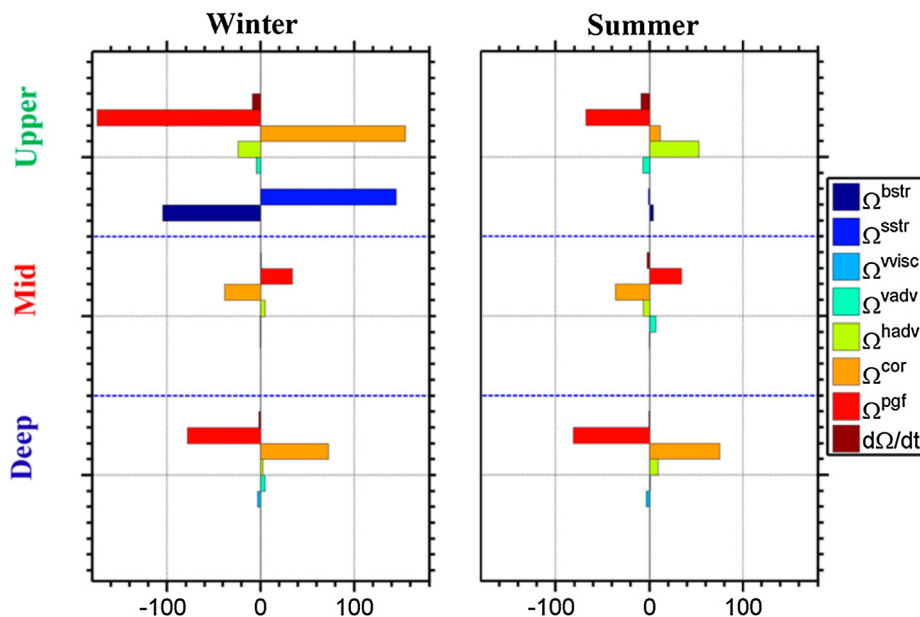


Fig. 6. Terms (m^3/s^2) of domain- and layer-integrated vorticity equation (Eq. (8)) in the upper, middle (mid), and deep layers during (left) winter and (right) summer. From Gan et al. (2016a).

Coriolis parameter. HNL and VNL are the horizontal and vertical non-linear advection terms. HVIS and VVIS are the horizontal and vertical viscous terms. Ω^{vis} can be further expressed as Ω^{sstr} (surface stress curl) $-\Omega^{\text{bstr}}$ (bottom stress curl) for the upper layer, where Ω^{sstr} represents the WSC. Ω^{pgf} is the bottom pressure torque that is formed by the interaction between baroclinicity induced pressure and the variable slope topography (Mertz and Wright, 1992).

According to divergence theorem, the domain-integrated Ω^{cor} can be expressed as the planetary vorticity flux through the surrounding straits, and represents the dominant external forcing:

$$\Omega^{\text{cor}} = - \int_{S_i} f \bar{u} dS_i - \int_{S_j} f \bar{v} dS_j \quad (9)$$

S_i and S_j are meridionally and zonally oriented sections.

Based on Eq. (8), the forcing mechanism of the CAC circulation is illustrated (Fig. 6). The vorticity dynamics in the upper layer show seasonality that during winter, the lateral vorticity flux (Ω^{cor}) and WSC (Ω^{sstr}) are the major sources of the cyclonic circulation and are mainly balanced by the bottom pressure torque (Ω^{pgf}) and bottom friction curl (Ω^{bstr}). During summer, the lateral planetary vorticity flux and the nonlinear advection effect (Ω^{cor} and Ω^{hadv}) are the major sources of positive vorticity for the relatively weak cyclonic circulation and also chiefly balanced by the bottom pressure torque (Ω^{pgf}). In the middle and deep layers, the Ω^{cor} is the main source of the respective anticyclonic and cyclonic circulations and are primarily balanced by the Ω^{pgf} . The magnitudes and the corresponding seasonality in the middle and deep layers are much smaller than that in the upper layer.

Eq. (8) is derived within a layer bounded by two geopotential surfaces. It directly reflects the balance of vorticity and circulation, because both are defined as perpendicular to the geopotential surfaces where we apply Stokes theorem (Eq. (1)). Eq. (8) has a different mathematical form from those based on the PV balance constraint (e.g. Yang et al., 2002; Zhu et al., 2017), but the two equations reveal constrains of circulation in different aspects, which are, however, consensus in the physical framework.

In the depth-integrated vorticity dynamics, the bottom pressure torque is the dominant response to the lateral planetary vorticity flux between different geopotential levels, while, in the PV balance constraint, the effect of the bottom pressure torque disappears and friction dissipates the PV flux between isopycnal surfaces. The bottom pressure measures the topographic effect for current steering, in which the

balance between the meridional flow and the bottom pressure torque results in the streamline broadly following the f/H contours. This allows the two constraints of PV and the depth-integrated vorticity to be consistently satisfied (Jackson et al., 2006). The simulations of gyre circulation and channel circulation by Jackson et al. (2006) also indicate that the topographic steering dictates the role of bottom friction in the PV distribution. Because the strong slope current along the western and northern SCS basin largely contributes to the basin circulation, the bottom pressure torque in Eq. (8) helps to understand the structural evolution of the slope current and explore the underlying dynamics that involve the current-slope interaction. Eq. (8) is defined in the geopotential coordinates, so Stokes theorem in Eq. (1) can be used to identify the layered circulation and diagnose the underlying dynamics.

When applying the geopotential partition to the abyssal closed SCS below the LS sill (~ 2500 m), there is no net direct horizontal mass and PV flux. However, as illustrated by Fig. 5, the depths of the isopycnal surfaces vary inside the basin, and the current along an isopycnal surface in the abyssal region induces the vertical motion/flux in the geopotential level. Consider the beta effect that the northern Coriolis parameter is relatively large. The deep intrusion through LS and the upwelling over the basin could induce a net vertical planetary vorticity flux (Eq. (13) below) to contribute to the deep layer cyclonic circulation. This is quantitatively consistent with Stommel and Arons (1959) that the mass source in the north and the sink over the basin would generate cyclonic circulation with a strong southward western boundary current. At the same time, the vertical advection also introduces the relative vorticity flux into the abyssal layer as shown in Eq. (8). Another possible forcing comes from the shear stress of the cyclonic circulation between 1500 m and 2500 m, which is directly driven by the deep intrusion through LS. The research of Yang and Pratt (2014) also considers the vertical motions between two layers and interfacial stress.

4. Vertical coupling among different layers

The theoretical works discussed above provide a framework for understanding the role of external forcing through the straits in forming the three-layer CAC circulation. However, besides external forcing, the vertical processes inside the basin dynamically couple the circulation in

the different layers and contributes to maintain the CAC circulation.

4.1. Layered model

The pioneering work of Luyten and Stommel (1986) provides a theoretical framework for the interaction between wind-driven circulation in the upper ocean and the thermohaline circulation below. The basic idea is that the upwelling of deep water into the upper ocean can be treated as a distributed source that compresses the upper layer. Thus, the upwelling of deep water associated with the thermohaline circulation plays a role similar to that of wind stress-induced Ekman pumping. Following this framework, Wang et al. (2012) investigate the dynamic influence of the thermohaline circulation on wind-driven circulation using a simple reduced gravity model. The momentum equation in the reduced gravity model that omits the time dependent, inertial and friction terms lead to the vorticity equation:

$$\beta h v = f(w_e - w_b), \quad (10)$$

where f is the Coriolis parameter; β is the meridional gradient of the Coriolis parameter; h is the upper-layer thickness; and v is the meridional velocity. w_e is the Ekman pumping velocity and w_b indicates the upwelling across the lower bound of the upper layer driven by the mixing from the deep ocean. The equation shows that a diapycnal velocity induced by mixing directly affects the upper layer wind-driven circulation. Therefore, to understand the surface wind-driven circulation in the SCS, the effects of the thermohaline circulation must be taken into consideration because the upwelling velocity from the deep part of the SCS is of the same order of magnitude as the typical Ekman pumping velocity. It should be noted that, in Wang et al. (2012), the upper layer wind-driven circulation and the deep thermohaline circulation are roughly separated by ~ 200 m, which is not same as the vertical separation of the CAC circulation.

With Eq. (10), the governing equation of the upper layer thickness is:

$$h^2(x, y) = h_e^2 - \frac{2f^2}{\beta g'} \int_x^{x_e} [w_e(x', y) - w_b(x', y)] dx' \quad (11)$$

where h_e is the thickness along the eastern boundary (x_e) of the basin. The squared upper layer thickness is proportional to the factor of f^2/β . Because f increases northward, but β slightly decreases with increasing latitude, the dynamic influence of thermohaline circulation on wind-driven circulation is larger in the northern SCS than in the southern SCS. With strong upwelling of deep water, the cyclonic gyre in the northern SCS weakens, but the anticyclonic gyre in the southern SCS intensifies in summer. However, the cyclonic gyres in both the southern and northern SCS weaken in winter (Fig. 7).

Similarly, it is also found that the vertical motions help to maintain the abyssal circulation, and the spatial distribution of the vertical mass flux significantly changes the abyssal circulation pattern (e.g. Marchal and Nycander, 2004; Katsman, 2006). Based on the reduced gravity model, the numerical experiments by Wang et al. (2018) show that, although the overall basin scale circulation pattern is mainly controlled by the overflow in the LS, the spatial pattern of upwelling has a strong impact on the regional structures of the deep water circulation in the interior basin. With downwelling occurring in the interior basin, the main deep circulation broadens and creates a branch flowing straight southward (Fig. 8).

Above attempts discussed so far, provide useful understandings on how circulation interacts among different layers. But they mainly consider one-way influences and a relatively idealized distribution of the vertical upwelling or downwelling is adopted in the investigation, so they could not capture the complete dynamic picture of the CAC circulation and do not fully investigate the interaction and coupling of the different layers.

Quan and Xue (2018) establish a three-layer reduced gravity model that includes entrainment, detrainment, and interfacial friction

between layers to explore the vertical coupling between the upper and middle layers. Generally, this layered-model illustrates the forcing mechanisms similar to those of Gan et al. (2016a) in which the WSC and external vorticity flux are the major driving forces of the layered circulation in the upper and middle layers (Fig. 9). In this layered model, the pressure gradient (PG) effect, which is the dominant response to the vorticity flux from lateral forcing or the WSC, represents the depth-integrated effect of the varying layer thicknesses. Thus, the varying thicknesses change the PG throughout the water column and link the circulation in the different layers. Based on the model results, the larger layer thickness variations occur mainly over the slope regions in the northern basin and along the western boundary east of Vietnam where there is a strong boundary current. In their layered model, the changes of the layer thicknesses (h_i) are determined by the combined effects of entrainment/detrainment and horizontal advection processes:

$$\frac{\partial h_i}{\partial t} = (w_{i(i+1)} - w_{(i-1)i}) - \nabla \cdot (h_i \vec{v}_i) \quad (12)$$

where $w_{i(i+1)}$ indicates the entrainment/detrainment between layers i and $i + 1$; \vec{v}_i means the horizontal velocity in layer i . The first term on the right hand side represents the change induced by the entrainment/detrainment (mixing effect) and the second term represents the change related to the horizontal transport (advective effect). By averaging the results in the whole basin over 10 years, it is found that the change induced by the entrainment/detrainment is about 20% of the total change and the rest part is due to advection.

In the CAC circulation, the strong slope current flows along the basin boundary and affects vertical coupling. However, as mentioned in Section 3.4, the calculation of the layer thickness is not reasonable in the boundary region where the density layer meets the slope topography. Furthermore, topographic steering effects may not be well resolved in a reduced gravity layered model. These factors may affect the diagnosis of vertical coupling.

4.2. Depth-integrated vorticity dynamics

Following the study of Gan et al. (2016a), Cai and Gan (2019) conduct a process-oriented study to investigate the coupled internal-external dynamics during the formation of the CAC circulation in the SCS. In Eq. (8), the Ω^{cor} that represents the net planetary flux through the surrounding straits can be divided into two terms:

$$\Omega^{cor} = - \int_A \left[\beta \int_{L_b}^{L_u} v dz \right] dA - \int_A \left[f \nabla \cdot \int_{L_b}^{L_u} \vec{v} dz \right] dA \quad (13)$$

The first term on the right hand side is the vorticity induced by the beta effect of the meridional velocity, and the second term illustrates the vortex stretching/squeezing induced by the divergence/convergence of the water. $f \nabla \cdot \int_{L_b}^{L_u} \vec{v} dz$ links with the horizontal motion and contributes to the momentum and vorticity exchange among different layers to develop and sustain the CAC circulation. Mathematically, it represents the net vertical planetary vorticity flux across the upper and lower boundaries of a layer. The upward transport crossing the upper/lower boundary can induce positive/negative vorticity into this layer and vice versa.

The idealized simulation in Cai and Gan (2019) shows that, in the upper layer, the input of planetary vorticity from LS in the northern part contributes mainly to the beta effect (VOR_BETA) rather than to the divergence effect (VOR_DIV) (Fig. 10a). Most of the intruding water in the upper layer from LS moves horizontally southward along the isobaths of the continental slope and exits the basin through the southern straits. This stronger meridional velocity leads to a larger beta effect. In the middle and lower layers where the basin is semi-closed, the magnitude of VOR_DIV is relatively large, and the vorticity input

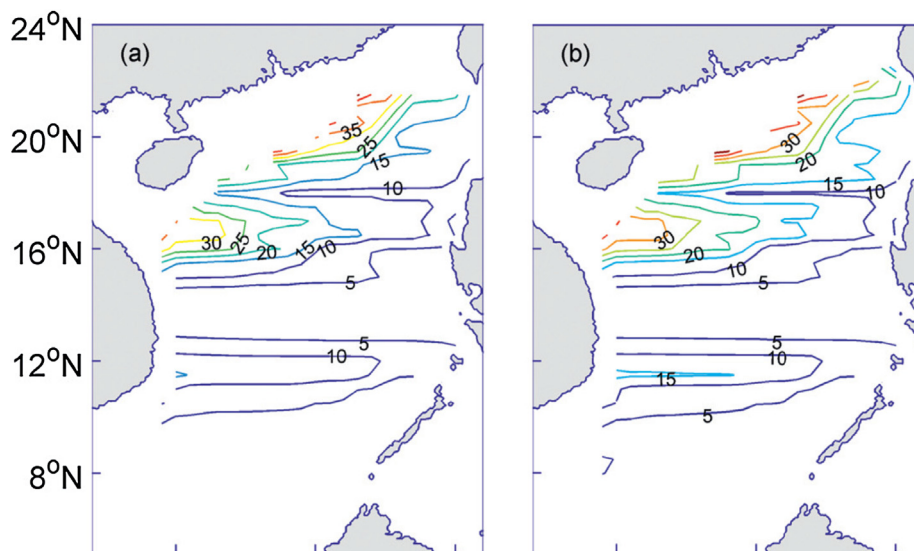


Fig. 7. The difference of thermocline depth (m) induced by upwelling from the deep ocean in (a) summer and (b) winter. From Wang et al. (2012).

induced by the vertical motion is the major response to the external vorticity flux. The time series of VOR_DIV in the different layers (Fig. 10b) shows that VOR_DIV in the upper and lower layers vary similarly, but with opposing signs, to that in the middle layer, except during very early stage. This suggests that the vertical motion and vorticity flux from the upper and lower layers produce negative VOR_DIV in the middle layer.

The vertical transport links the circulation in the three layers and acts as the source or sink of vorticity, particularly in forming and sustaining the middle- and lower-layer circulation. The vertical transport between the different layers mainly occurs over the slope because of the cross-slope motion due to flow-slope interaction (Gan et al., 2013) that includes the along-isobath bottom friction and PGF (Fig. 11). Therefore,

the intrinsic interactions between the strong slope current and topography are the major contributors to the cross-isobath motions over the slope.

5. Summary and prospects

(a) Summary

We summarize the forcing mechanisms of the CAC circulation in Fig. 12 based on our current understanding on the layered circulation in the SCS.

The formation of the CAC circulation is attributed to the combined effects of surface wind forcing, layered lateral external flow, and the

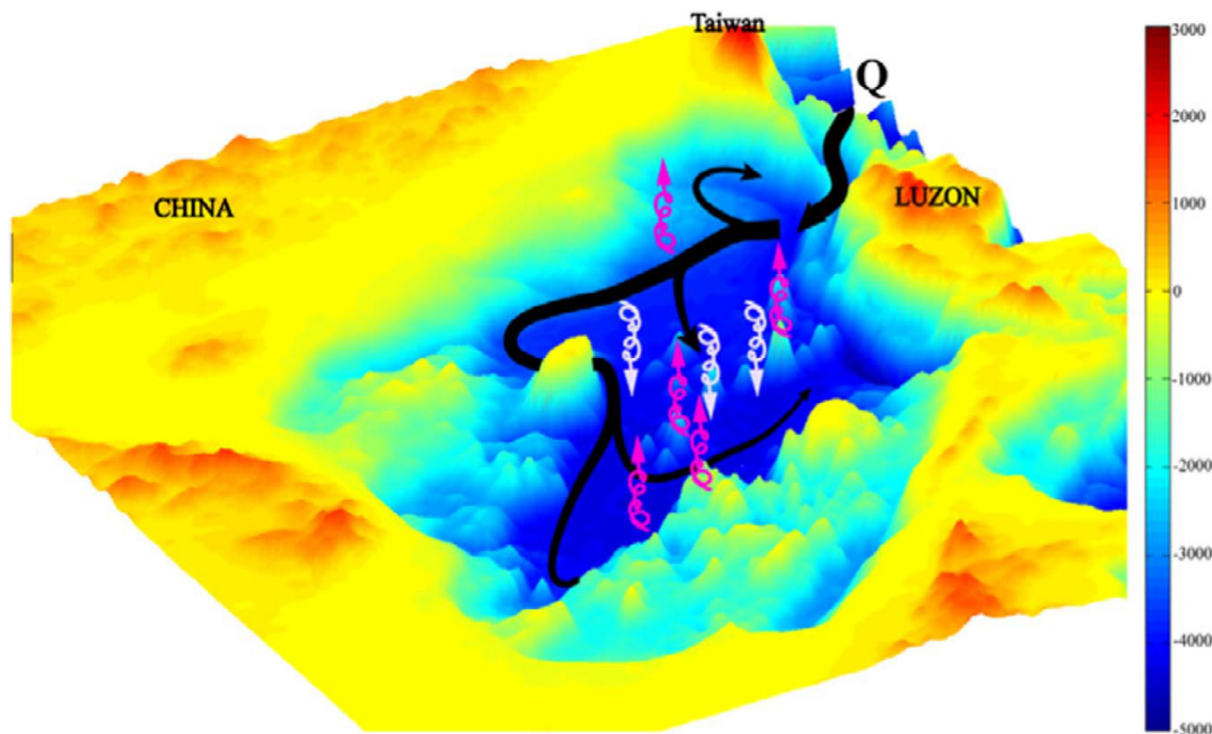


Fig. 8. Schematic circulation (black contour) showing the SCS deep circulation pattern. The deep layer receives a net volume flux, Q at the LS that is balanced by diapycnal velocity, w^* . The gray dashed circulation and diapycnal velocity are speculated. From Wang et al. (2018).

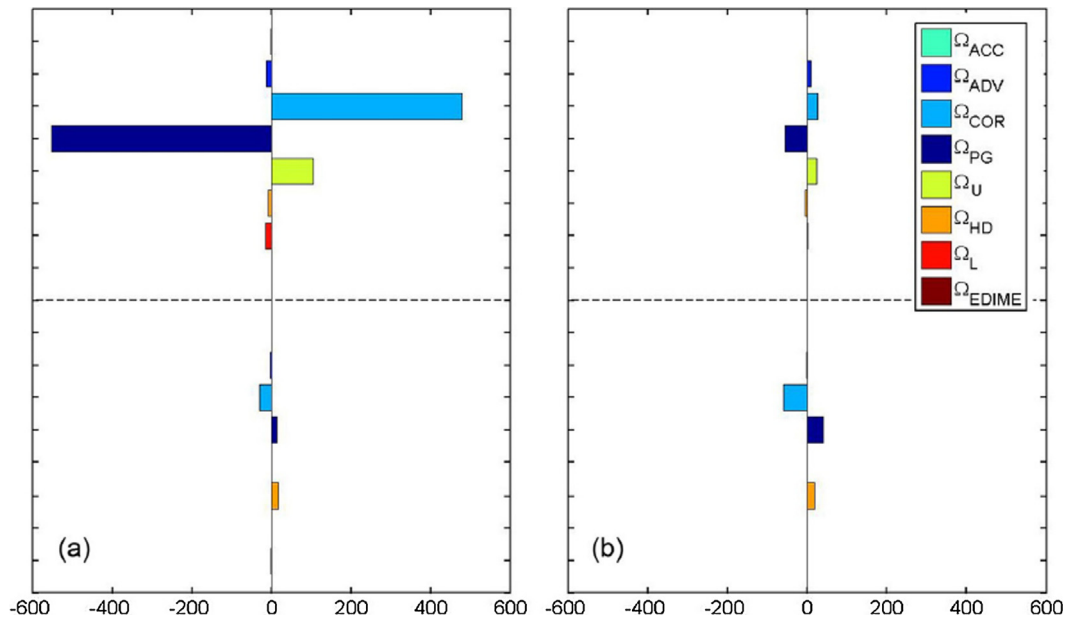


Fig. 9. Terms (m^3/s^2) in the domain- and layer-integrated vorticity equation for (a) winter and (b) summer from the control run. The two partitions separated by the black dashed line correspond to the upper (1st plus 2nd) and middle (3rd) layer in the SCS (model), respectively. Note that the yellow bar represents either the WS curl for the upper layer or the interface friction curl at the upper interface for the middle layer. The red bar represents the sum of the interface friction curl and bottom friction curl at the lower interface of the layer. From Quan and Xue (2018). (For interpretation of the references to color in this figure legend, the reader is referred to the web version of this article.)

intrinsic coupling among different layers. The surface wind forcing contributes mainly to the upper layer circulation while the layered structure of the CAC circulation is largely controlled by the external inflow-outflow-inflow through LS. The upper layer inflow is induced by the Kuroshio Current intrusion, which is closely linked with the current system in the tropical western Pacific Ocean. The deep layer inflow and middle layer outflow are driven by the cross LS baroclinic pressure gradient induced by the density differences between the SCS basin and the Pacific Ocean. The mixing rate in the deep SCS is several orders larger than that of the Pacific Ocean, and the contrasting mixing intensity on both sides of LS sustains the density differences across LS and drives deep water exchanges.

The three layer inflow-outflow-inflow through LS produces the inflow-outflux-influx of planetary vorticity into the SCS to form the CAC circulation, and is predominantly balanced by the interaction between the CAC flow and bottom topography. The abyssal basin is closed

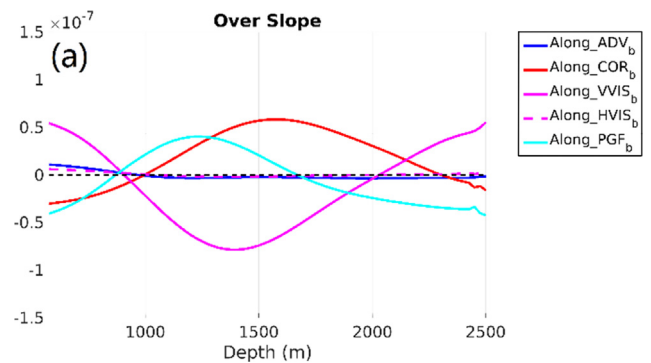


Fig. 11. Terms (m^2/s^2) of along-isobath momentum balance times the bottom topography slope. The terms are integrated over the bottom 50 m and averaged along the strip over the slope as a function of depth. From Cai and Gan (2019).

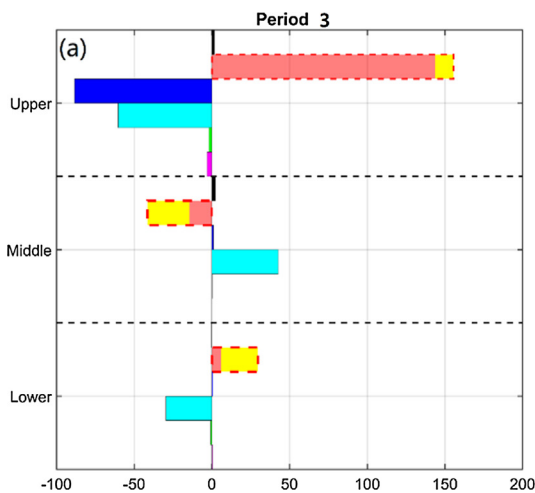
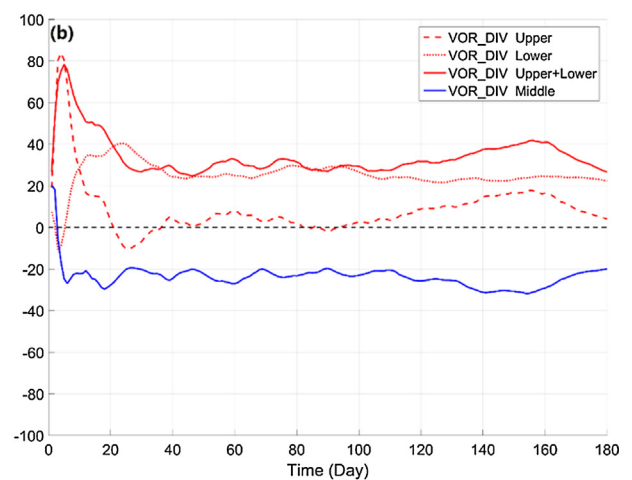


Fig. 10. Terms (m^3/s^2) in depth-integrated vorticity dynamics in the upper, middle, and lower layers. (b) Time series of VOR_DIV averaged over the respective upper, middle, and lower layers. From Cai and Gan (2019).



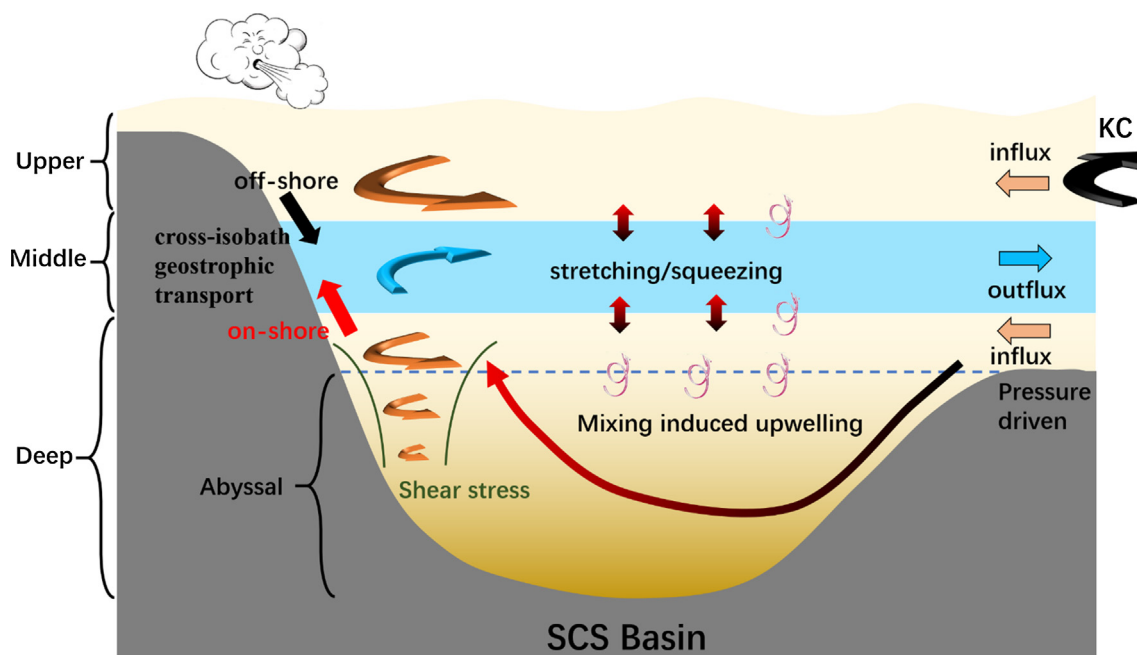


Fig. 12. Conceptual diagram showing the forcing mechanisms of the CAC circulation in the SCS.

without direct influence from horizontal external forcing, however, the net vertical vorticity flux caused by cascading of the deep intrusion water and the upward transport inside the basin, and the interfacial shear stress from the cyclonic circulation between 1500 m and 2500 m, which is directly driven by deep intrusion through LS, could possibly generate the abyssal cyclonic circulation. The generated internal layered circulation, in turn, affects and modulates the layered current structure in LS.

The vertical processes including mixing and advection dynamically link the circulation in the different layers, which play a crucial role in sustaining the CAC circulation. The vertical coupling occurs mainly over the slope regions because of the cross-slope motion that is largely controlled by the bottom along-isobath pressure gradient and is induced by the interaction between the background circulation and slope topography.

In the middle and deep layers, the vertical vorticity flux is the major response to the external forcing and its spatial pattern has a strong impact on the regional structures of the circulation, while the vertical vorticity flux has a relatively smaller influence on the upper layer circulation. Through vertical coupling, the changes in the surface wind forcing and lateral external forcing can be transmitted through the water column and affect the entire layered circulation.

(b) Prospects

The detailed structures and the variability of the basin circulation in the middle, deep, and abyssal layers in the SCS are largely unclear because of the limited number of direct observations. Long-term and synchronous observed and high-resolution topographic datasets need to be promoted, especially over the northern, western, and southern basin slope regions where the intensified boundary current and strong vertical coupling are located. Having these data will unveil the multi-scale processes associated with the basin circulation and enrich the knowledge of the forcing mechanisms proposed in previous studies.

The general CAC circulation is driven by external forcing, but the detailed structure of basin circulation/slope current is also modulated by internal adjustments and vertical coupling. The vertical partition of the domain-averaged vorticity is not the same as the LS transport pattern because the circulation extends vertically as it flows along the slope's isobaths. The intrinsic baroclinic adjustment of the slope current

as it interacts with topography should be explored to have an overall understanding of the three-dimensional structure of the circulation. The vertical coupling illustrated in earlier studies is mainly based on an idealized configuration. The complex distribution and variability of the vertical vorticity/momentum exchange among the different layers are needed to fully reveal how the CAC circulation is formed and maintained.

The deep intrusion and middle layer outflow in LS are largely related to the baroclinic pressure gradient set up by the density difference between the Pacific Ocean and the SCS, which also is, in turn, affected by the circulation in both the SCS and Pacific Ocean. The coupled dynamic system that includes background circulation and mixing in the SCS basin and Pacific Ocean need to be investigated together to reveal the formation of the three-layer inflow-outflow-inflow structure in LS. Lastly, the contribution of mixing and advection processes in forming and maintaining the full depth CAC circulation need further quantitative investigation.

Acknowledgement

This research was supported by the Key Research Project of the National Science Foundation (41930539), the National (China) Key Basic Research Development Program (2015CB954004) and the Hong Kong Research Grants Council (GRF16204915 and GRF 16206516). We are also grateful for the support of The National Supercomputing Center of Tianjin and Guangzhou.

References:

- Alford, M.H., Peacock, T., MacKinnon, J., Nash, J., Buijsman, M., Centurioni, L., Chao, S., Chang, M., Farmer, D., Fringer, O., Fu, K., Gallacher, P., Graber, H., Helfrich, K., Jachec, S., Jackson, C., Klymak, J., Ko, D., Jan, S., Johnston, T., Legg, S., Lee, I., Lien, R., Mercier, M., Moum, J., Musgrave, R., Park, J., Pickering, A., Pinkel, R., Rainville, L., Ramp, S., Rudnick, D., Sarkar, S., Scotti, A., Simmons, H., Laurent, L., Venayagamoorthy, S., Wang, Y., Wang, J., Yang, Y., Paluszkiwicz, T., Tang, T., 2015. The formation and fate of internal waves in the South China Sea. *Nature* 521, 65–69. <https://doi.org/10.1038/nature14399>.
- Anderson, D., Gill, A., 1975. Spin-up of a stratified ocean, with applications to upwelling. *Deep Sea Res. Oceanogr. Abstr.* 22 (9), 583–596. [https://doi.org/10.1016/0011-7471\(75\)90046-7](https://doi.org/10.1016/0011-7471(75)90046-7).
- Bayler, E., Liu, Z., 2008. Basin-scale wind-forced dynamics of the seasonal southern South China Sea gyre. *J. Geophys. Res.* 113 (C7), 1–22. <https://doi.org/10.1029/2007JC004519>.
- Cai, S., Long, X., Wang, S., 2007. A model study of the summer Southeast Vietnam

- offshore current in the southern South China Sea. *Continental Shelf Res.* 27 (18), 2357–2372. <https://doi.org/10.1016/j.csr.2007.06.002>.
- Cai, S., He, Y., 2010. Association of the Sulu Sea surface circulation with the South China Sea. *J. Mar. Syst.* 81, 335–340. <https://doi.org/10.1016/j.marsys.2010.02.010>.
- Cai, Z., Gan, J., 2017. Formation and dynamics of a long-lived eddy-train in the South China Sea: a modeling study. *J. Phys. Oceanogr.* <https://doi.org/10.1175/JPO-D-17-0002.1>.
- Cai, Z., Gan, J., 2019. Coupled external-internal dynamics of layered circulation in the South China Sea: a modeling study. *J. Geophys. Res.* 124. <https://doi.org/10.1029/2019JC014962>.
- Cane, M., 1989. A mathematical note on Kawase's study of the deep-ocean circulation. *J. Phys. Oceanogr.* 19 (4), 548–550. [https://doi.org/10.1175/1520-0485\(1989\)019<0548:AMNOKS>2.0.CO;2](https://doi.org/10.1175/1520-0485(1989)019<0548:AMNOKS>2.0.CO;2).
- Caruso, M., Gawarkiewicz, G., Beardsley, R., 2006. Interannual variability of the Kuroshio intrusion in the South China Sea. *J. Oceanogr.* 62, 559–575. <https://doi.org/10.1007/s10872-006-0076-0>.
- Cessi, P., Louazel, S., 2001. Decadal oceanic response to stochastic wind forcing. *J. Phys. Oceanogr.* 31 (10), 3020–3029. [https://doi.org/10.1175/1520-0485\(2001\)031<3020:DORTSW>2.0.CO;2](https://doi.org/10.1175/1520-0485(2001)031<3020:DORTSW>2.0.CO;2).
- Chang, M., Lien, R., Tang, T., Asaro, E., Yang, Y., 2006. Energy flux of nonlinear internal waves in northern South China Sea. *Geophys. Res. Lett.* 33, L03607. <https://doi.org/10.1029/2005GL025196>.
- Chen, C., Huang, M., 1996. A mid-depth front separating the South China Sea water and the Philippine sea water. *J. Oceanogr.* 52 (1), 17–25. <https://doi.org/10.1007/BF02236530>.
- Chern, C., Wang, J., 1998. A numerical study of the summertime flow around the Luzon Strait. *J. Oceanogr.* 54, 53–64. <https://doi.org/10.1007/BF02744381>.
- Chern, C., Wang, J., 2003. Numerical study of the upper-layer circulation in the South China Sea. *J. Oceanogr.* 59, 11–24. <https://doi.org/10.1023/A:1022899920215>.
- Chu, P., Edmons, N., Fan, C., 1999. Dynamical mechanisms for the South China Sea seasonal circulation and thermohaline variabilities. *J. Phys. Oceanogr.* 29 (11), 2971–2989. [https://doi.org/10.1175/1520-0485\(1999\)029<2971:DMFTSC>2.0.CO;2](https://doi.org/10.1175/1520-0485(1999)029<2971:DMFTSC>2.0.CO;2).
- Chu, P., Li, R., 2000. South China Sea isopycnal-surface circulation. *J. Phys. Oceanogr.* 30, 2419–2438. [https://doi.org/10.1175/1520-0485\(2000\)030<2419:SCSISC>2.0.CO;2](https://doi.org/10.1175/1520-0485(2000)030<2419:SCSISC>2.0.CO;2).
- Fang, G., Kwok, Y., Yu, K., Zhu, Y., 1999. Numerical simulation of principal tidal constituents in the South China Sea, Gulf of Tonkin and Gulf of Thailand. *Continental Shelf Res.* 19, 845–869. [https://doi.org/10.1016/S0278-4343\(99\)00002-3](https://doi.org/10.1016/S0278-4343(99)00002-3).
- Fang, G., Susanto, D., Soesilo, I., 2005. A note on the South China Sea shallow interocean circulation. *Adv. Atmos. Sci.* 22, 946–954. <https://doi.org/10.1007/BF02918693>.
- Fang, G., Wang, Y., Wei, Z., 2009. Interocean circulation and heat and freshwater budgets of the South China Sea based on a numerical model. *Dyn. Atmos. Oceans* 47 (1), 55–72. <https://doi.org/10.1016/j.dynatmoce.2008.09.003>.
- Fang, G., Wang, G., Fang, Y., Fang, W., 2012. A review on the South China Sea western boundary current. *Acta Oceanol. Sin.* 31 (5), 1–10. <https://doi.org/10.1007/s13131-012-0231-y>.
- Gan, J., Li, H., Curchitser, E., Haidvogel, D., 2006. Modeling South China Sea circulation: response to seasonal forcing regimes. *J. Geophys. Res. Oceans* 111 (C6). <https://doi.org/10.1029/2005JC003298>.
- Gan, J., Liu, Z., Hui, C., 2016a. A three-layer alternating spinning circulation in the South China Sea. *J. Phys. Oceanogr.* 46 (8), 2309–2315. <https://doi.org/10.1175/JPO-D-16-0044.1>.
- Gan, J., Liu, Z., Liang, L., 2016b. Numerical modeling of intrinsically and extrinsically forced seasonal circulation in the China Seas: a kinematic study. *J. Geophys. Res. Oceans* 121 (7), 4697–4715. <https://doi.org/10.1002/2016JC011800>.
- Gan, J., Ho, H., Liang, L., 2013. Dynamics of intensified downwelling circulation over a widened shelf in the northeastern South China Sea. *J. Phys. Oceanogr.* 43 (1), 80–94. <https://doi.org/10.1175/JPO-D-12-02.1>.
- Gan, J., Qu, T., 2008. Coastal jet separation and associated flow variability in the south-western South China Sea. *Deep Sea Res.* 55, 1–19. <https://doi.org/10.1016/j.dsr.2007.09.008>.
- Guo, C., Chen, X., 2014. A review of internal solitary wave dynamics in the northern South China Sea. *Prog. Oceanogr.* 121, 7–23. <https://doi.org/10.1016/j.pocean.2013.04.002>.
- Ho, C., Kuo, N., Zheng, Q., Soong, Y., 2000. Dynamically active areas in the South China Sea detected from TOPEX/POSEIDON satellite altimeter data. *Remote Sens. Environ.* 71, 320–328. [https://doi.org/10.1016/S0034-4257\(99\)00094-2](https://doi.org/10.1016/S0034-4257(99)00094-2).
- Hsin, Y.C., Wu, C., Chao, S., 2012. An updated examination of the Luzon Strait transport. *J. Geophys. Res.* 117 (C3), 1–18. <https://doi.org/10.1029/2011JC007714>.
- Hu, J., Kawamura, H., Hong, H., Qi, Y., 2000. A review on the currents in the South China Sea: seasonal circulation, South China Sea warm current and Kuroshio intrusion. *J. Oceanogr.* 56 (6), 607–624. <https://doi.org/10.1023/A:101117531252>.
- Jackson, L., Hughes, C., Williams, R., 2006. Topographic control of basin and channel flows: The role of bottom pressure torques and friction. *J. Phys. Oceanogr.* 36 (9), 1786–1805. <https://doi.org/10.1175/JPO2936.1>.
- Jan, S., Lien, R., Ting, C., 2008. Numerical study of baroclinic tides in Luzon Strait. *J. Oceanogr.* 64, 789–802. <https://doi.org/10.1007/s10872-008-0066-5>.
- Jan, S., Chern, C., Wang, J., Chiou, M., 2012. Generation and propagation of baroclinic tides modified by the Kuroshio in the Luzon Strait. *J. Geophys. Res. Oceans* 117 (C2). <https://doi.org/10.1029/2011JC007229>.
- Johnson, H., Marshall, D., 2002. A theory for the surface Atlantic response to thermohaline variability. *J. Phys. Oceanogr.* 32, 1121–1132. [https://doi.org/10.1175/1520-0485\(2002\)032<1121:ATFTSA>2.0.CO;2](https://doi.org/10.1175/1520-0485(2002)032<1121:ATFTSA>2.0.CO;2).
- Kashino, Y., Espana, N., Syamsudin, F., Richards, K., Jensen, T., Dutrieux, P., Ishida, A., 2009. Observations of the North Equatorial Current, Mindanao Current, and Kuroshio Current system during the 2006/07 El Niño and 2007/08 La Niña. *J. Oceanogr.* 65, 325–333. <https://doi.org/10.1007/s10872-009-0030-z>.
- Katsman, C., 2006. Impacts of localized mixing and topography on the stationary abyssal circulation. *J. Phys. Oceanogr.* 36 (8), 1660–1671. <https://doi.org/10.1175/JPO2925.1>.
- Kantha, L., Tierney, C., 1997. Global baroclinic tides. *Prog. Oceanogr.* 40, 163–178. [https://doi.org/10.1016/S0079-6611\(97\)00028-1](https://doi.org/10.1016/S0079-6611(97)00028-1).
- Kawase, M., 1987. Establishment of deep ocean circulation driven by deep-water production. *J. Phys. Oceanogr.* 17 (12), 2294–2317. [https://doi.org/10.1175/1520-0485\(1987\)017<2294:EODOCD>2.0.CO;2](https://doi.org/10.1175/1520-0485(1987)017<2294:EODOCD>2.0.CO;2).
- Kim, Y., Qu, T., Jensen, T., Miyama, T., Mitsudera, H., Kang, H., Ishida, A., 2004. Seasonal and interannual variations of the North Equatorial Current bifurcation in a high-resolution OGCM. *J. Geophys. Res. Oceans* 109, 109. <https://doi.org/10.1029/2003JC002013>.
- Lan, J., Wang, Y., Cui, F., Zhang, N., 2015. Seasonal variation in the South China Sea deep circulation. *J. Geophys. Res. Oceans* 120 (3), 1682–1690. <https://doi.org/10.1002/2014JC010413>.
- Lan, J., Zhang, N., Wang, Y., 2013. On the dynamics of the South China Sea deep circulation. *J. Geophys. Res. Oceans* 118 (3), 1206–1210. <https://doi.org/10.1002/jgrc.20104>.
- Lebedev, K., Yaremchuk, M., 2000. A diagnostic study of the Indonesian Throughflow. *J. Geophys. Res. Oceans* 105, 11243–11258. <https://doi.org/10.1029/2000JC900015>.
- Li, L., Qu, T., 2006. Thermohaline circulation in the deep South China Sea basin inferred from oxygen distributions. *J. Geophys. Res. Oceans* 111 (C5). <https://doi.org/10.1029/2005JC003164>.
- Liang, W., Tang, T., Yang, Y., Ko, M., Chuang, W., 2003. Upper-ocean currents around Taiwan. *Deep Sea Res Part II: Topical Stud. Oceanogr.* 50, 1085–1105. [https://doi.org/10.1016/S0967-0645\(03\)00011-0](https://doi.org/10.1016/S0967-0645(03)00011-0).
- Liu, J., He, Y., Wang, D., Liu, T., Cai, S., 2015. Observed enhanced internal tides in winter near the Luzon Strait. *J. Geophys. Res. Oceans* 120, 6637–6652. <https://doi.org/10.1002/2015JC011131>.
- Liu, Q., Yang, H., Liu, Z., 2001. Seasonal features of the Sverdrup circulation in the South China Sea. *Prog. Natural Sci.* 11, 202–206.
- Liu, Q., Kaneko, A., Su, J., 2008. Recent progress in studies of the South China Sea circulation. *J. Oceanogr.* 64 (5), 753–762. <https://doi.org/10.1007/s10872-008-0063-8>.
- Liu, W., Xie, X., 1999. Space based observations of the seasonal changes of south Asian monsoons and oceanic responses. *Geophys. Res. Lett.* 26 (10), 1473–1476. <https://doi.org/10.1029/1999GL900289>.
- Liu, Z. H., Yang, and Q. Liu (2001). Regional dynamics of seasonal variability in the South China Sea. *J. Phys. Oceanogr.*, 31(1): 272-284, [https://doi.org/10.1175/1520-0485\(2001\)031<0272:RDOSVI>2.0.CO;2](https://doi.org/10.1175/1520-0485(2001)031<0272:RDOSVI>2.0.CO;2).
- Liu, Z., Gan, J., 2016. Open boundary conditions for tidally and subtidally forced circulation in a limited-area coastal model using the Regional Ocean Modeling System (ROMS). *J. Geophys. Res. Oceans* 121 (8), 6184–6203. <https://doi.org/10.1002/2016JC011975>.
- Liu, Z., Gan, J., 2017. Three-dimensional pathways of water masses in the South China Sea: A modeling study. *J. Geophys. Res. Oceans* 122 (7), 6039–6054. <https://doi.org/10.1002/2016JC012511>.
- Luyten, J., Stommel, H., 1986. Gyres driven by combined wind and buoyancy flux. *J. Phys. Oceanogr.* 16 (9), 1551–1560. [https://doi.org/10.1175/1520-0485\(1986\)016<1551:GDBCWA>2.0.CO;2](https://doi.org/10.1175/1520-0485(1986)016<1551:GDBCWA>2.0.CO;2).
- Marchal, O., Nycander, J., 2004. Nonuniform upwelling in a shallow-water model of the Antarctic Bottom Water in the Brazil Basin. *J. Phys. Oceanogr.* 34 (11), 2492–2513. <https://doi.org/10.1175/JPO2643.1>.
- Marshall, D., Johnson, H., 2013. Propagation of meridional circulation anomalies along western and eastern boundaries. *J. Phys. Oceanogr.* 43, 2699–2717. <https://doi.org/10.1175/JPO-D-13-0134.1>.
- Mertz, G., Wright, D., 1992. Interpretations of the JEBAR term. *J. Phys. Oceanogr.* 22 (3), 301–305. [https://doi.org/10.1175/1520-0485\(1992\)022<0301:IOJTJ>2.0.CO;2](https://doi.org/10.1175/1520-0485(1992)022<0301:IOJTJ>2.0.CO;2).
- Metzger, E., Hurlburt, H., 1996. Coupled dynamics of the South China Sea, the Sulu Sea, and the Pacific Ocean. *J. Geophys. Res. Oceans* 101 (C5), 12331–12352. <https://doi.org/10.1029/95JC03861>.
- Metzger, E., 2003. Upper ocean sensitivity to wind forcing in the South China Sea. *J. Oceanogr.* 59, 783–798. <https://doi.org/10.1023/B:JOCE.0000009570.41358.c5>.
- Nan, F., Xue, H., Chai, F., Wang, D., Yu, F., Shi, M., Guo, P., Xiu, P., 2013. Weakening of the Kuroshio intrusion into the South China Sea over the past two decades. *J. Climate* 26 (20), 8097–8110. <https://doi.org/10.1175/JCLI-D-12-00315.1>.
- Nan, F., Xue, H., Yu, F., 2015. Kuroshio intrusion into the South China Sea: A review. *Prog. Oceanogr.* 137, 314–333. <https://doi.org/10.1016/j.pocean.2014.05.012>.
- Nitani, H. (1972). On the deep and bottom waters in the Japan Sea. In: *Research in Hydrography and Oceanography* (ed. D. Shoji), Hydrographic Department of Japan, p. 151–201.
- Niwa, Y., Hibiya, T., 2004. Three-dimensional numerical simulation of M2 internal tides in the East China Sea. *J. Geophys. Res. Oceans* 109, C04027. <https://doi.org/10.1029/2003JC001923>.
- Pedlosky, J., 1996. *Ocean Circulation Theory*. Springer-Verlag, pp. 453.
- Pedlosky, J., 1998. *Ocean Circulation Theory*, 2nd ed., Springer, Berlin, pp. 453.
- Qiu, B., Lukas, R., 1996. Seasonal and interannual variability of the North Equatorial Current, the Mindanao Current, and the Kuroshio along the Pacific western boundary. *J. Geophys. Res. Oceans* 101 (C5), 12315–12330. <https://doi.org/10.1029/95JC03204>.
- Qu, T., Mitsudera, H., Yamagata, T., 1998. On the western boundary currents in the Philippine Sea. *J. Geophys. Res. Oceans* 103, 7537–7548. <https://doi.org/10.1029/98JC00263>.
- Qu, T., 2000. Upper-layer circulation in the South China Sea. *J. Phys. Oceanogr.* 30 (6), 1450–1460. [https://doi.org/10.1175/1520-0485\(2000\)030<1450:ULCITS>2.0.CO;2](https://doi.org/10.1175/1520-0485(2000)030<1450:ULCITS>2.0.CO;2).
- Qu, T.D., Mitsudera, H., Yamagata, T., 2000. Intrusion of the North Pacific waters into the South China Sea. *J. Geophys. Res.* 105 (C3), 6415–6424. <https://doi.org/10.1029/1999JC900323>.
- Qu, T., Lukas, R., 2003. The bifurcation of the North Equatorial Current in the Pacific. *J. Phys. Oceanogr.* 33, 5–18. [https://doi.org/10.1175/1520-0485\(2003\)033<0005:TBOTNE>2.0.CO;2](https://doi.org/10.1175/1520-0485(2003)033<0005:TBOTNE>2.0.CO;2).

- Qu, T., Kim, Y., Yaremchuk, M., 2004. Can Luzon Strait transport play a role in conveying the impact of ENSO to the South China Sea? *J. Clim.* 17, 3644–3656. [https://doi.org/10.1175/1520-0442\(2004\)017<3644:CLSTPA>2.0.CO;2](https://doi.org/10.1175/1520-0442(2004)017<3644:CLSTPA>2.0.CO;2).
- Qu, T., Du, Y., Meyers, G., Ishida, A., Wang, D., 2005. Connecting the tropical Pacific with Indian Ocean through South China Sea. *Geophys. Res. Lett.* 32, L24609. <https://doi.org/10.1029/2005GL024698>.
- Qu, T., Girtan, J., Whitehead, J., 2006. Deepwater overflow through Luzon Strait. *J. Geophys. Res. Oceans* 111 (C1). <https://doi.org/10.1029/2005JC003139>.
- Qu Song, T.Y., Yamagata, T., 2009. An introduction to the South China Sea throughflow: its dynamics, variability, and application for climate. *Dyn. Atmos. Oceans* 47 (1), 3–14. <https://doi.org/10.1016/j.dynatmoce.2008.05.001>.
- Quan, X., Xue, H., 2018. Layered model and insights into the vertical coupling of the South China Sea circulation in the upper and middle layers. *Ocean Model.* 129, 75–92. <https://doi.org/10.1016/j.ocemod.2018.06.006>.
- Quan, Q.H., Xue, H., Qin, X., Zeng, Peng, S., 2016. Features and variability of the South China Sea western boundary current from 1992 to 2011. *Ocean Dyn.* 66, 1–16. <https://doi.org/10.1007/s10236-016-0951-1>.
- Rong, Z., Liu, Y., Zong, H., Cheng, Y., 2007. Interannual sea level variability in the South China Sea and its response to ENSO. *Global Planet. Change* 55, 257–272. <https://doi.org/10.1016/j.gloplacha.2006.08.001>.
- Shaw, P., Chao, S., 1994. Surface circulation in the South China Sea. *Deep Sea Res Part I: Oceanographic Res. Papers* 41 (11), 1663–1683. [https://doi.org/10.1016/0967-0637\(94\)90067-1](https://doi.org/10.1016/0967-0637(94)90067-1).
- Shaw, P., Chao, S., Fu, L., 1999. Sea surface height variations in the South China Sea from satellite altimetry. *Oceanol. Acta* 22 (1), 1–17. [https://doi.org/10.1016/S0399-1784\(99\)80028-0](https://doi.org/10.1016/S0399-1784(99)80028-0).
- Shu, Y., Xue, H., Wang, D., Chai, F., Xie, Q., Yao, J., Xiao, J., 2014. Meridional overturning circulation in the South China Sea envisioned from the high-resolution global reanalysis data GLBa0. *J. Geophys. Res.* 119 (5), 3012–3028. <https://doi.org/10.1002/2013JC009583>.
- Song, Y., 2006. Estimation of interbasin transport using ocean bottom pressure: theory and model for Asian marginal seas. *J. Geophys. Res.* 111, C11S19. <https://doi.org/10.1029/2005JC003189>.
- Stommel, H. and A. Arons (1959). On the abyssal circulation of the world ocean—I. Stationary planetary flow patterns on a sphere. *Deep Sea Res.* (1953) 6: 140–154.
- Su, J., 2004. Overview of the South China Sea circulation and its influence on the coastal physical oceanography outside the Pearl River Estuary. *Contin. Shelf Res.* 24 (16), 1745–1760. <https://doi.org/10.1016/j.csr.2004.06.005>.
- Tian, J., Qu, T., 2012. Advances in research on the deep South China Sea circulation. *Chinese Sci. Bull.* 57 (24), 3115–3120. <https://doi.org/10.1007/s11434-012-5269-x>.
- Tian, J., Yang, Q., Liang, X., Xie, L., Hu, D., Wang, F., Qu, T., 2006. Observation of Luzon Strait transport. *Geophys. Res. Lett.* 33 (L19607), 1–6. <https://doi.org/10.1029/2006GL026272>.
- Toole, J., Zou, E., Millard, R., 1988. On the circulation of the upper waters in the western equatorial Pacific Ocean. *Deep Sea Res Part A: Oceanogr. Res. Papers* 35, 1451–1482. [https://doi.org/10.1016/0198-0149\(88\)90097-0](https://doi.org/10.1016/0198-0149(88)90097-0).
- Tian, J., Yang, Q., Zhao, W., 2009. Enhanced diapycnal mixing in the South China Sea. *J. Phys. Oceanogr.* 39, 3191–3203. <https://doi.org/10.1175/2009JPO3899.1>.
- Toole, J., Millard, R., Wang, Z., Pu, S., 1990. Observations of the Pacific North Equatorial Current bifurcation at the Philippine coast. *J. Phys. Oceanogr.* 20, 307–318. [https://doi.org/10.1175/1520-0485\(1990\)020<0307:OOPNE>2.0.CO;2](https://doi.org/10.1175/1520-0485(1990)020<0307:OOPNE>2.0.CO;2).
- Tozuka, T., Kagimoto, T., Masumoto, Y., Yamagata, T., 2002. Simulated multiscale variations in the western tropical Pacific: the Mindanao Dome revisited. *J. Phys. Oceanogr.* 32, 1338–1359. [https://doi.org/10.1175/1520-0485\(2002\)032<1338:SMVITW>2.0.CO;2](https://doi.org/10.1175/1520-0485(2002)032<1338:SMVITW>2.0.CO;2).
- Wang, A., Du, Y., Peng, S., Liu, K., Huang, R., 2018. Deep water characteristics and circulation in the South China Sea. *Deep Sea Res Part I: Oceanogr. Res. Papers* 134, 55–63. <https://doi.org/10.1016/j.dsr.2018.02.003>.
- Wang, D., Q. Wang, S. Cai, X. Shang, S. Peng, Y. Peng, J. Xie, X. Xie, Z. Zhang, Z. Liu, J. Lan, D. Chen, H. Xue, G. Wang, J. Gan, X. Xie, R. Zhang, H. Chen, and Q. Yang (2019). Progress on multi-scale dynamics processes in middle and deep layers of the South China Sea (in Chinese). *Science China-Earth Sciences, SSTE-2019-0118*.
- Wang, D., Wang, W., Shi, P., Guo, P., Gan, Z., 2003. Establishment and adjustment of monsoon-driven circulation in the South China Sea. *Sci. China, Ser. D Earth Sci.* 46 (2), 173–181. <https://doi.org/10.1360/03yd9016>.
- Wang, D., Liu, Q., Huang, R., Du, Y., Qu, T., 2006a. Interannual variability of the South China Sea throughflow inferred from wind data and an ocean data assimilation product. *Geophys. Res. Lett.* 33, L14605. <https://doi.org/10.1029/2006GL026316>.
- Wang, G., Chen, D., Su, J., 2006b. Generation and life cycle of the dipole in the South China Sea summer circulation. *J. Geophys. Res.* 111 (C06002), 1–9. <https://doi.org/10.1029/2005JC003314>.
- Wang, G., Huang, R., Su, J., Chen, D., 2012. The effects of thermohaline circulation on wind-driven circulation in the South China Sea. *J. Phys. Oceanogr.* 42 (12), 2283–2296. <https://doi.org/10.1175/JPO-D-11-0227.1>.
- Wang, G., Xie, S., Qu, T., Huang, R., 2011. Deep South China Sea circulation. *Geophys. Res. Lett.* 38 (L05601), 1–6. <https://doi.org/10.1029/2010GL046626>.
- Wang, X., S. Peng, Z. Liu, R. Huang, Y. Qian, and Y. Li (2016). Tidal mixing in the South China Sea: an estimate based on the internal tide energetics. *J. Phys. Oceanogr.*, 46(1): 107–124. <https://doi.org/10.1175/JPO-D-15-0082.1>.
- Wang, X., Liu, Z., Peng, S., 2017. Impact of tidal mixing on water mass transformation and circulation in the South China Sea. *J. Phys. Oceanogr.* 47 (2), 419–432. <https://doi.org/10.1175/JPO-D-16-0171.1>.
- Wang, Y., Fang, G., Wei, Z., Qiao, F., Chen, H., 2006c. Interannual variation of the South China Sea circulation and its relation to El Niño, as seen from a variable grid global ocean model. *J. Geophys. Res. Oceans* 111 (C11). <https://doi.org/10.1029/2005JC003269>.
- Wei, Z., Fang, G., Xu, T., Wang, Y., Lian, Z., 2016. Seasonal variability of the isopycnal surface circulation in the South China Sea derived from a variable-grid global ocean circulation model. *Acta Oceanol. Sin.* 35 (1), 11–20. <https://doi.org/10.1007/s13131-016-0791-3>.
- Wijffels, S., Firing, E., Toole, J., 1995. The mean structure and variability of the Mindanao Current at 8 N. *J. Geophys. Res. Oceans* 100, 18421–18435. <https://doi.org/10.1029/95JC01347>.
- Wu, C., Shaw, P., Chao, S., 1998. Seasonal and interannual variations in the velocity field of the South China Sea. *J. Oceanogr.* 54 (4), 361–372. <https://doi.org/10.1007/BF02742620>.
- Wu, C., Hsin, Y., 2012. The forcing mechanism leading to the Kuroshio intrusion into the South China Sea. *J. Geophys. Res. Oceans* 117 (C7). <https://doi.org/10.1029/2012JC007968>.
- Wyrtki, K. (1961). Scientific results of marine investigations of the South China Sea and the Gulf of Thailand, 1959–1961. *Naga Report 2*, Univ. Calif., Scripps Institute of Oceanogr.
- Xie, Q., Xiao, J., Wang, D., Yu, Y., 2013. Analysis of deep-layer and bottom circulations in the South China Sea based on eight quasi-global ocean model outputs. *Chin. Sci. Bull.* 58, 4000–4011. <https://doi.org/10.1007/s11434-013-5791-5>.
- Xu, F., Oey, L., 2015. Seasonal SSH variability of the Northern South China Sea. *J. Phys. Oceanogr.* 45, 1595–1609. <https://doi.org/10.1175/JPO-D-14-0193.1>.
- Xu, F., Oey, L., 2014. State analysis using the Local Ensemble Transform Kalman Filter (LETKF) and the three-layer circulation structure of the Luzon Strait and the South China Sea. *Ocean Dyn.* 64 (6), 905–923. <https://doi.org/10.1007/s10236-014-0720-y>.
- Xue, H.F., Chai, N., Pettigrew, D., Xu, M. Shi, Xu, J., 2004. Kuroshio intrusion and the circulation in the South China Sea. *J. Geophys. Res.* 109 (C2), 1–14. <https://doi.org/10.1029/2002JC001724>.
- Yang, J., 1999. A linkage between decadal climate variations in the Labrador Sea and the tropical Atlantic Ocean. *Geophys. Res. Lett.* 26 (8), 1023–1026. <https://doi.org/10.1029/1999GL900181>.
- Yang, H., Q. Liu, Z. Liu, D. Wang, and X. Liu (2002). A general circulation model study of the dynamics of the upper ocean circulation of the South China Sea. *J. Geophys. Res.*, 107(C7): 22-21-22-14, doi:10.1029/2001JC001084.
- Yang, J., Pratt, L.J., 2014. Some dynamical constraints on upstream pathways of the Denmark Strait overflow. *J. Phys. Oceanogr.* 44, 3033–3053. <https://doi.org/10.1175/JPO-D-13-0227.1>.
- Yang, J., Price, J., 2000. Water-mass formation and potential vorticity balance in an abyssal ocean circulation. *J. Mar. Res.* 58 (5), 789–808. <https://doi.org/10.1357/002224000321358918>.
- Yang, Q., Tian, J., Zhao, W., 2010. Observation of Luzon Strait transport in summer 2007. *Deep-Sea Res. I* 57, 670–676. <https://doi.org/10.1016/j.dsr.2010.02.004>.
- Yang, Q., Tian, J., Zhao, W., Liang, X., Zhou, L., 2014. Observations of turbulence on the shelf and slope of northern south china sea. *Deep Sea Res Part I: Oceanogr. Res. Papers* 87, 43–52. <https://doi.org/10.1016/j.dsr.2014.02.006>.
- Yang, Q., Zhao, W., Liang, X., Tian, J., 2016. Three-dimensional distribution of turbulent mixing in the South China Sea. *J. Phys. Oceanogr.* 46, 769–788. <https://doi.org/10.1175/JPO-D-14-0220.1>.
- Yang, Q., Nikurashin, M., Sasaki, H., Sun, H., Tian, J., 2019. Dissipation of mesoscale eddies and its contribution to mixing in the northern South China Sea. *Sci. Rep.* 9 (1). <https://doi.org/10.1038/s41598-018-36610-x>.
- Yaremchuk, M., Qu, T., 2004. Seasonal variability of the large-scale currents near the coast of the Philippines. *J. Phys. Oceanogr.* 34, 844–855. [https://doi.org/10.1175/1520-0485\(2004\)034<0844:SVOTLC>2.0.CO;2](https://doi.org/10.1175/1520-0485(2004)034<0844:SVOTLC>2.0.CO;2).
- Yaremchuk, M., McCreary, J., Yu, Z., Furue, R., 2009. The South China Sea throughflow retrieved from climatological data. *J. Phys. Oceanogr.* 39, 753–767. <https://doi.org/10.1175/2008JPO3955.1>.
- Yuan, D., 2002. A numerical study of the South China Sea deep circulation and its relation to the Luzon Strait transport. *Acta Oceanol. Sin.* 21 (2), 187–202.
- Zhao, W., Hou, Y., Qi, P., Le, K., Li, M., 2009. The effects of monsoons and connectivity of South China Sea on the seasonal variations of water exchange in the Luzon Strait. *J. Hydrodyn.* 21, 263–270. [https://doi.org/10.1016/S1001-6058\(08\)60144-4](https://doi.org/10.1016/S1001-6058(08)60144-4).
- Zhao, W., Zhou, C., Tian, J., Yang, Q., Wang, B., Xie, L., Qu, T., 2014. Deep water circulation in the Luzon Strait. *J. Geophys. Res. Oceans* 119 (2), 790–804. <https://doi.org/10.1002/2013JC009587>.
- Zhao, Z., 2014. Internal tide radiation from the Luzon Strait. *J. Geophys. Res. Ocean.* 119, 5434–5448. <https://doi.org/10.1002/2014JC010014>.
- Zhang, Z., Zhao, W., Liu, Q., 2010. Sub-seasonal variability of Luzon Strait transport in a high resolution global model. *Acta Oceanol. Sin.* 29 (3), 9–17. <https://doi.org/10.1007/s13131-010-0032-0>.
- Zhou, C., Zhao, W., Tian, J., Zhao, X., Zhu, Y., Yang, Q., Qu, T., 2017. Deep western boundary current in the South China Sea. *Sci. Rep.* 7 (1), 9303. <https://doi.org/10.1038/s41598-017-09436-2>.
- Zhu, Y., Sun, J., Wang, Y., Li, S., Xu, T., Wei, Z., Qu, T., 2019. Overview of the multi-layer circulation in the South China Sea. *Prog. Oceanogr.* 175, 171–182. <https://doi.org/10.1016/j.poccean.2019.04.001>.
- Zhu, Y., Sun, J., Wang, Y., Wei, Z., Yang, D., Qu, T., 2017. Effect of potential vorticity flux on the circulation in the South China Sea. *J. Geophys. Res. Oceans* 122 (8), 6454–6469. <https://doi.org/10.1002/2016JC012375>.
- Zu, T., J. Gan, and S. Y. Erofeeva (2008). Numerical study of the tide and tidal dynamics in the South China Sea, *Deep-Sea Res. I*, doi: 10.1016/j.dsr.2007.10.007.